Title
Advancements in conventional and 3D printed feed spacers in membrane modules

Authors
Qian, Xin
Anvari, Arezou
Hoek, Eric MV
et al.

Publication Date
2023-06-01

DOI
10.1016/j.desal.2023.116518

Advancements in Conventional and 3D Printed Feed Spacers in Membrane Modules

By

Xin Qian[1], Arezou Anvari[2], Eric M.V. Hoek[2,3], Jeffrey R. McCutcheon[1,*]

[1] Department of Chemical & Biomolecular Engineering, University of Connecticut, Storrs, CT

[2] Department of Civil & Environmental Engineering, Institute of the Environment & Sustainability, California NanoSystems Institute, University of California, Los Angeles (UCLA), Los Angeles, CA, USA

[3] Energy Storage & Distributed Resources Division, Lawrence Berkeley National Lab, Berkeley, CA, USA

Submitted to

Desalination

March 21, 2024

* Corresponding author: jeffrey.mccutcheon@uconn.edu; +1.860.486.4601

Table of Contents

Abstract

Flat-sheet and spiral-wound modules are used for gas separation, pervaporation, reverse osmosis, nanofiltration, ultrafiltration, microfiltration, electro-dialysis, electro-deionization, membrane distillation and forward osmosis membrane separations. Feed channel spacers are an integral part of both module types – providing mechanical support for a cross-flow channel through the module and, in most cases, promoting mixing to enhance mass transfer, which helps reduce concentration polarization and fouling. However, enhanced mass transfer comes at a cost of increased hydraulic pressure losses and stagnant zones wherever a spacer filament touches a membrane surface; these stagnant zones exacerbate membrane fouling and make cleaning more difficult. Efforts to improve feed spacer performance largely focus on adjusting the chemistry or geometry of the spacer to mitigate these challenges. Additive manufacturing, a.k.a., 3D printing, offers new degrees of freedom in feed spacer design and production, which opens up a new area of research in membrane technology. This review critically assesses the peer-reviewed literature on conventional net- or mesh-style feed spacers in addition to various novel spacer geometries and chemistries produced via 3D printing. We further review and evaluate conventional spacer manufacturing methods and discuss advantages and disadvantages of 3D printed spacers.

Keywords

Spiral-wound; Plate-and-frame; Feed spacer; Fouling; Scaling; Pressure drop; 3D printing

1. Introduction

Polymeric membranes for liquid and gas separations are packaged into modules comprising three primary form factors: flat-sheet membranes in either (1) spiral-wound elements (SWEs) or (2) flat-sheet plate-and-frame (P&F) stacks as well as (3) cylindrical membranes in the form of bundled hollow-fiber, capillary and tubular modules [1,2]. Key to the manufacturing and operation of the first two module types is the inclusion of spacers on both sides of the membrane to hold flow channels open, support the membranes under operating conditions, and enhance mass transfer near the membrane interfaces. Spacers are used in all SWE and P&F membrane applications, and are of particular interest for aqueous separations such as reverse osmosis (RO), nanofiltration (NF), ultrafiltration (UF), forward osmosis (FO), membrane distillation (MD), pervaporation (PV), and ion exchange (IX) membrane processes [1,2]. Herein, we focus our critical review on SWE and P&F form factors, both of which require a feed spacer to provide mechanical separation between neighboring membrane flat-sheets.

Spacers are used in both the feed and permeate channels of membrane elements. Feed channel spaces are used to hold the channel open to flow and to improve mixing and mass transfer through the reduction of concentration polarization (CP) [3–6]. Permeate channel spacers hold the channel open to enable permeate to leave the module, but may have a role in mixing in membrane contactor processes (e.g., forward osmosis, electro-dialysis). For applications where there is a transmembrane hydraulic pressure drop (e.g., RO, NF, UF, MF), the permeate spacer is also designed to adequately support the membrane under pressure to prevent channel collapse. In these applications, permeate spacers are typically made thinner and with a less porous structure [7–9].

The research community has focused far more on feed spacers than permeate spacers. This in part because the feed channel is where the more complex mass transfer related phenomena occur (i.e., fouling, CP). Fouling mitigation in particular has been a research priority in the membrane field for many years, and many have identified the spacer as a design feature of elements that can be changed to mitigate fouling [i.e., fouling, CP]. This has resulted in a vast majority of the spacer design research to be relegated to feed spacers. Much of this work is conceptualized in NF/RO desalination and UF protein separation applications.

Regardless of where the spacer is within the module, one of the primary drawbacks of spacers is the creation of pressure drop along the channel. This pressure drop is particularly problematic in high crossflow when attempting to minimize CP and fouling [10]. This pressure drop may be exacerbated by fouling, which may clog up spacers [11]. Numerous studies have focused on improving the hydrodynamic design of conventional net-type feed spacers to: (1) maximize mixing and turbulence [12], (2) minimize the pressure drop [13,14], (3) prevent the dead zones to mitigate membrane fouling [15,16] and (4) minimize the contact and compressive stress on membrane surface to avoid damaging the membrane selective layer [17].

Although these studies succeeded in improving some aspects of feed spacer performance, most of them only considered net-type feed spacer geometries. While computational fluid dynamics (CFD) studies have shown that feed spacer geometries that go beyond net-type spacers could theoretically improve spacer performance [18–20], these complex structures are not manufacturable using conventional techniques. Conventional manufacturing of net-type spacers such as extrusion, molding, vacuum foaming or filament gluing lack resolution, accuracy and conformational versatility in forming intricate spacer shapes.

Emerging additive manufacturing approaches (i.e. 3D printing) has offered additional degrees of freedom in designing and manufacturing feed spacers. 3D printing enables the development of exotic structures that would be impossible to manufacturing using traditional extrusion methods. As these printing methods continue to evolve and exhibit improved speed, pricing and resolution, new opportunities around spacer design have emerged in recent years.

Other review articles [21–24] on 3D printing in membranes have provided a broad discussion on 3D printed membranes, spacers and elements without a focus on spacer manufacturing and metrics evaluation. We believe this review will provide more focused insight on applications of 3D printing approaches specifically for spacers. We provide this review in the context of how these new manufacturable designs have enabled improved fouling resistance, enhanced mass transfer and reduced pressure drop. This review will also compare different spacer manufacturing techniques in terms of performance benefits and commercial viability. This review will be limited in scope to liquid filtration applications with flat-sheet P&F and SWE type membrane modules.

2. Attempts to Improve Spacer Performance

Before specifically addressing the use of additive manufacturing in building new spacers, we provide a brief assessment of the research categories for feed spacer improvement research. We assess both material and geometry selection below.

2.1. Material Improvement

Much of the research in identifying new spacer material has been an attempt to address fouling issues associated with feed spacers in membrane modules. Results have concluded, somewhat counterintuitively, that spacers may in fact exacerbate fouling near the spacer itself due to stagnant zone formation [10,25]. A number of previous studies have sought to improve the fouling resistance of spacers by modifying the spacer material or surface. Many of these studies, summarized in Table 1, have attempted to functionalize the spacer surfaces, particularly for biofouling.

Alleviating biofouling through spacer modification has largely focused on surface chemistries designed to inhibit the bacterial activity and/or tpo improve the spacer hydrophilicity. Many of these studies explored the use of metal or metal oxides coatings that greatly improved the long term permeate flux and reduced the foulant attachment [26–29]. Hydrophilic polymers have also been functionalized on spacer surfaces either by grafting [30–32] or plasma treatment [33,34]. Carbon-based materials such as CNT or graphene oxide have been considered due to their demonstrated biotoxicity [35]. However, most of the surface treatments were performed after the manufacturing of spacer. Such approaches could result in weak surface attachment or heterogeneous distribution of the coating material. These challenges may limit lifetime and functionality of the modification.

Table 1. Spacer surface modifications and their effect in performance improvement.

Spacer material	Spacer modification	Application	Effect	Reference
N/A (from FilmTec^{TM} SW30-2514)	Surface coating with silver nanoparticles via silver nitrate solution immersion	RO	Lower flux decay rate. Higher (95%) TDS rejection than unmodified membrane and spacer. Ability to mitigate biofouling.	[Yang, 2009]
Polypropylene	Surface coating with silver nanoparticles via sonochemical deposition	UF	Complete bacteria reduction after 3hrs in static liquid condition. Only 2.4% biofilm attachment during long-term crossflow test.	[Ronen, 2015]
Polypropylene	Surface coating with zinc oxide nanoparticles via sonochemical deposition	UF	99.9% bacteria reduction after 3hrs in static liquid condition. Almost no accumulation of biofilm in crossflow test.	[Ronen, 2013]
Polypropylene	Surface coating with zinc oxide nanorods via chemical bath deposition	UF	Much lower bacteria attachment and higher permeability than clean PP spacer in both flow through mode and crossflow condition.	[Thamaraiselvan, 2019]
Polypropylene	Surface grafting with spacer arm	RO	An order of magnitude lower bacterial attachment than the	[Hausman, 2009]

	(glycidyl methacrylate) and Cu(II) charged metal chelating ligands		virgin PP spacer.	
Polypropylene	Sputter coating with silver, copper or gold with different thickness	NF/RO	Thicker spacer and low linear flow velocities reduced the pressure drop increase in a long period of time. Coating could delay the fouling rate but does not prevent fouling.	[Araújo, 2012]
Polypropylene	Surface modification by polydopamine coating and poly(ethylene glycol) grafting	NF/UF	Over 99.9% reduction in BSA and over 75% lower intensity of bacteria in static liquid condition. Did not inhibit biofouling in long-term biofouling test in MFS.	[Miller, 2012]
Polypropylene	Surface functionalization by diethylene glycol ether via plasma polymerization	RO	Spacers modified at certain plasma energy density could yield reduced biomass attachment.	[Reid, 2014]
High density polyethylene /polypropylene (80/20 wt %)	Surface functionalization by poly(sulfobetaine methacrylate) (pSBMA) zwitterionic polymer via plasma polymerization	RO	Approximately 70% reduced bacterial attachment in 24hr static liquid suspension. Did not significantly inhibit biofouling in continuous tests in MFS.	[Jabłońska, 2020]
Polypropylene	Surface modification by pQAs via ATRP	UF	Better ‘short distance’ localized antibacterial activity but worse ‘long distance’ capacity than nanosilver coated spacers.	[Ronen, 2016]
Polypropylene	Surface coating by polydopamine, polydopamine-graft-poly(ethylene glycol) or copper	UF/NF/RO	Copper coated spacers reduced pressure drop and biomass accumulation, but hydrophilic polymer modification did not.	[Araújo, 2012]
Polypropylene	Surface functionalization by silver, SiO_2 nanoparticles,	RO	Silver coated spacers outperformed other spacers in terms of biofouling control.	[Rice, 2018]

	$TMPSi\text{-}TiO_2$ nanoparticles or graphene oxide.			
Polypropylene-CNTs	Blending CNT with PP spacer via injection molding	RO	High loading of CNTs filler induced stronger antifouling against BSA. Hybrid spacers showed 7-8 times lower foulant attachment than plain PP spacer.	[Kitano, 2019]
Titanium metal, plastic	Dip coating plastic spacer with GNPs to make it conductive	MF/UF/NF/RO	The conductive spacers could help the in-situ cleaning of membrane to mitigate foulants and improve the flux in an electrochemical system.	[Abid, 2017]
Polyamide	TPMS (Gyr-tCLP hybrid) spacers coated by fluorinated silica (FS) and a variety of graphene oxide or graphene nanosheets	MD	FS surface coating resulted in the largest antiscaling enhancement with a 74% lower scalant attachment on the spacer and 60% lower scalant attachment on the membrane than the pristine uncoated spacer.	[Thomas, 2021]

2.2. Spacer Structural Improvement

A number of studies have attempted to explore the “optimum” net-type spacer filament thickness, spacing and angle. Details of these efforts and the relevant spacer performance improvement are listed in Table 2. Generally, the change of flow pattern should induce changes in mass transfer, pressure drop and CP. Some of the design features include filament spacing (distance between two consecutive filaments), filament height (diameter of filament), hydrodynamic angle (interior angle between two adjacent spacer filaments relative to feed flow) and flow attack angle (the angle between the flow and hydrodynamic angle). Larger filament spacing could elongate the streamline between two filaments, leading to a lower critical Reynolds number to achieve vortex shedding [36]. Thicker filaments usually result in large wakes of fluid past transverse filaments [37] and aid the formation of secondary recirculation region able to disrupt the boundary layer and enhance mass transfer [12]. According to Park et al. [38], spacer thickness is an important factor in reducing differential pressure and fouling. A 28-mil feed spacer exhibited 78% higher normalized differential pressure (NDP) increment than the 34-mil spacer in a 659 hr RO filtration test. Furthermore, the thicker spacer distributed the fouling load more evenly, enhanced membrane cleaning efficiency and prolonged the membrane lifecycle [38]. In terms of the hydrodynamic angle and flow attack angle, a proper combination of these angles with filament size and spacing could reach a balance between mass transfer, pressure drop and fouling [39–41]. Novel cross section profiles of filaments, such as oval, wing-like or triangle shaped spacers, have been considered for reducing pressure drop and fouling or improving mass transfer [19,20,42]. Studies [43] have evaluated the transverse filament position in the feed channel, where submerged type of filament alignment (all transverse filaments are located at the feed channel bottom) showed best flux and biofouling reduction at the cost of larger pressure drop. Spacer filaments could also intertwine into different woven states. Gu et al. [3] demonstrated that the fully woven spacers (where filaments are all interlaced together) provided higher flux and lower concentration polarization than other shapes although with slightly higher pressure drop compared with other woven states.

Simple geometrical adjustments, such as a change of filament location, varying filament size and mesh length, altering hydrodynamic and flow attack angle are achievable for conventionally extruded net-type or ladder spacers. These modifications are also assessable by most CFD software packages. Complex spacer geometries such as multi-layer spacers [44], twisted filaments [4] and spacers with triply periodic minimal surface (TPMS) structures [5,45–48], are exceedingly difficult with conventional manufacturing methods. Therefore, most recent studies have adopted 3D printing to fabricate novel spacer structures.

Table 2. Spacer structural optimizations and their effect on spacer performance

Spacer type	Structural modification	Method	Effect	Reference
Net-type spacers	Hydrodynamic angle, transverse filament size and location	Crossflow test	Hydrodynamic angle of 90˚ yielded 50% higher flux than 0˚. Flux increased by up to 9% by increasing filament size from 0.7mm to 1.07mm.	[Da Costa, 1994]
Net-type spacers	Hydrodynamic angle, mesh size, thickness, filament diameter and voidage	Crossflow test, pressure drop and mass transfer models	40% voidage and 50˚-120˚ hydrodynamic angle attributed to optimal pressure drop and mass transfer at low crossflow velocities. 60%-70% voidage and 70˚-90˚ hydrodynamic angle reduced pressure drop and enhanced mass transfer at high crossflow velocities.	[Da Costa, 1994]
Net-type spacers	Hydrodynamic angle (β)	Crossflow test	At low flow rate, the spacer with 80˚ hydrodynamic angle had lowest overall cost. At high flow rate, the spacer with 45˚-60˚ hydrodynamic angle had lowest overall cost.	[Da Costa, 1991]
Net-type spacers	Transverse filament location,	CFD	Submerged spacer was desired for better mass transfer. Short filament spacing resulted	[Cao, 2001]

	filament spacing		in higher mass transfer at the cost of pressure drop.	
Ladder-type spacers	Filament spacing, filament size	CFD	Larger filament spacing elongated the streamline between two filaments, decreased critical Re number and slightly reduced the friction factor. Larger filament size led to larger recirculation area, enhanced mass transfer but augmented friction factor.	[Geraldes, 2002]
Ladder-type spacers	Transverse filament location	CFD, crossflow test	Concentration polarization of cavity spacers is independent of the distance to channel inlet. Higher concentration polarization was observed with longer channel length for non-cavity spacers (transverse filaments opposite to membrane).	[Geraldes, 2002]
Net-type spacers	Ratio of filament spacing to channel height (λ/a), flow attack angle (α)	Wind tunnel test	Flow attack angle could alter the pressure drop by a factor of 30 and change the mass transfer by 2.7 times. A proper combination of these geometric parameters could balance mass transfer, mixing and energy costs.	[Zimmerer, 1996]
Net-type spacers	λ/a, channel length, α and β	CFD, flat channel electrode experiment	The optimal spacer geometry is set at $\lambda/a=4$, $\alpha=30^{\circ}$ and $\beta=120^{\circ}$, which led to the optimal Sherwood number (Sh) in a broad range of power number (Pn).	[Li, 2002], [Li, 2004]
Net-type spacers	Filament spacing to diameter ratio (L/D), β	Direct numerical simulations, crossflow test	Local shear stress and pressure drop decreased with increasing L/D and increased with higher β.	[Koutsou, 2007]
Net-type spacers	α	CFD	45° flow attack angle generated higher mass transfer and lower pressure drop than 90° orientation.	[Fimbres-Weihs, 2007]
Net-type spacers	α	Direct observation through the membrane (DOTM)	0° flow attack angle yielded the best fouling performance.	[Neal, 2003]
Zigzag spacers	Filament cross section, tilt angle	CFD	Enhanced mass transfer, lowest pressure drop, and decreased fouling were achieved if oval	[Amokrane, 2016]

			spacers were tilted at 20°.	
N/A	Filament cross section	CFD	Triangular spacers had higher concentration minimization ability and pressure drop. Circular spacers had the lowest energy consumption.	[Ahmad, 2005]
Net-type spacers	Filament cross section	CFD	Concave (spherical) spacer could drastically reduce the pressure drop and simultaneously maintained high strain rate compared with other spacer configurations.	[Ranade, 2006]
Ladder-type spacers	Transverse filament location	A 2D numerical model based on fundamental transport equations	The submerged spacers exhibited lowest biomass accumulation, lowest flux decline and salt concentration in permeate but with highest pressure drop.	[Radu, 2010]
Ladder-type spacers, diamond type spacers	Filament diameter, mesh length and arrangement of the spacer filaments	Crossflow test	The 3-layer spacer had an improvement in flux, mass transfer and concentration polarization compared with 2-layer spacer, but it also came with higher pressure loss.	[Schwinge, 2004]
Net-type spacers	Spacer layers, filament shape, λ/a, α and β	CFD	The optimal multi-layer spacer showed 30% higher Sherwood number and only 40% of the power consumption compared with optimal non-woven spacer.	[Li, 2005]
Net-type spacers	Spacer layers, filament shape, filament diameter, spacer height, α and β	Electrodialysis measurements	Thinner middle layer could reduce the power consumption by 30 time while still maintained 20% higher mass transfer than 2-layer spacers.	[Balster, 2006]
Net-type spacers	Filament configuration, α and β	CFD	Fully woven spacers, although with a slightly higher pressure drop, provided higher flux and lower concentration polarization than other shapes. Lower β induced lower flux and larger concentration polarization. Pressure drop was very sensitive to α.	[Gu, 2017]
Ladder-type, triple, wavy and submerged spacers	Spacer configuration	CFD	Ladder-type spacers had the highest spacer configuration efficacy (SCE) when the Re is lower than 120 while the wavy spacers took priority in SCE at higher turbulence.	[Kavianipour, 2017]
Helically	Filament shape	Forced	The helical shaped spacer	[Fritzmann

microstructured spacers		crossflow test in submerged membrane bioreactors (MBR)	improved the critical flux of membrane by 100% and reduced fouling by a factor of 7.5	, 2013]
TPMS spacers	TPMS shapes	Crossflow BWRO and UF tests	The incorporation of TPMS spacers enhanced flux, reduced biofouling and pressure drop.	[Sreedhar, 2018]

2.3. Conventional Spacer Manufacturing

In the last few decades, polymers have been processed into different shapes via different processing techniques [49–52]. Most feed channel spacers are made of thermoplastics, which are commonly extruded or molded. However, these conventional processing techniques limit spacer geometries to conventional ladder- and net-type structures. Novel or exotic spacer geometries are not processable using extrusion and molding complex geometries with small feature sizes is costly. This section mainly discusses the most widely used conventional processes for fabricating spacers and the limitations of these methods. Details of each conventional manufacturing technique are summarized in Table 3.

Table 3. Conventional spacer manufacturing techniques, material, process and limitations.

Manufacturing technique	Material	Process	Limitations	References
Extrusion	Thermoplastics, metal, ceramic, composite	Feed the material into a hopper, compress, heat and mix the material in the extruder, which subsequently	Low resolution. Only able to form net-type spacers. Low accuracy and precision due to die swell.	[Grida, 2003], [Anand, 1980], [Mount, 2017], [Piau, 1990],

		extrudes the material through a die to form spacer filaments. After extrusion, the filaments are usually welded, glued or bonded together.	Inhomogeneity and defects in filaments.	[Kissi, 1997], [Ahmad, 1995], [Schwinge, 2004], [Smythe, 2020]
Injection molding	Thermoplastics, composite	The plastic pellets are compressed and molten in a barrel and subsequently injected into a mold under high pressure. The mold then cools down and ejects the spacer out.	Low resolution, accuracy and precision. Low manufacturing speed.	[Singh, 2017], [Khosravani, 2019]
Vacuum forming	Thermoplastics	Melts and shapes thermoplastic film sheet in a mold to produce desired products.	Low resolution, accuracy and precision. Low manufacturing speed.	[Sawada, 1989], [Leite, 2018]

2.3.1. Extrusion

Extrusion is a widely used method in processing polymeric, ceramic, metal and composite materials into a variety of structures such as films, rods and tubes. Feed channel spacer filaments are usually manufactured by either barrel extruder or rotary extruder. The most common extrusion process involves feeding the polymer into a hopper, heating and mixing the material in the extruder, which subsequently extrudes the material through a die to form desired structure. The spacer filament usually exhibits some degrees of twisting due to the shear force during extrusion. The first layer of extruded filaments are placed in parallel and additional layers are usually welded [53], glued [54] or fusion bonded [55] at a specific angle with the first layer to form the spacer. This angle determines the shape of the mesh (e.g., diamond or square netted spacers). Extrusion can also be used to form composite spacer filaments by mixing filler material with polymer and can be made into a continuous process.

2.3.2. Injection Molding

Injection molding is an important manufacturing process capable of producing large quantities of plastic parts with high dimensional tolerance at high speed. Injection molding is considered as a near net-shape manufacturing process that does not require further finishing process [56]. In injection molding process, the plastic pellets are compressed and molten in a barrel and subsequently injected into a mold under high pressure. The molten plastic is kept in the mold at high pressure for a certain period of time to shape and solidify the product while the mold is cooling down. The product is then ejected out of the mold before new plastics are injected into the mold. Depending on the actual material and processing requirement, a whole injection molding cycle usually takes 2 seconds to 2 minutes. Due to low costs, fast production and minimal wastage, injection molding has been used for producing metal [57], ceramic [58], composite [59] and powder [60] materials. Injection molding has also been used for producing net-shaped spacers [35].

3. 3D Printing in Spacer Manufacturing

3.1. 3D Printing Techniques Relevant to Spacer Manufacturing

3D printing is become a popular topic in membrane fabrication [61–64]. In this section, we review the 3D printing techniques relevant to spacer manufacturing. Most 3D printing techniques manufacture product layer by layer which enables the forming of delicate and complex morphological features such as a variety of intricate structures proposed in novel feed spacer designs. Additionally, most 3D printing methods (with a few exceptions) can form spacers with a high-quality surface finish, which is important for fouling and pressure drop control during filtration. Basic illustrations of the relevant printing techniques discussed in this review are illustrated in Figure 1. Detailed descriptions of these techniques, their advantages and disadvantages have been illustrated in our previous paper on 3D printed membranes [65].

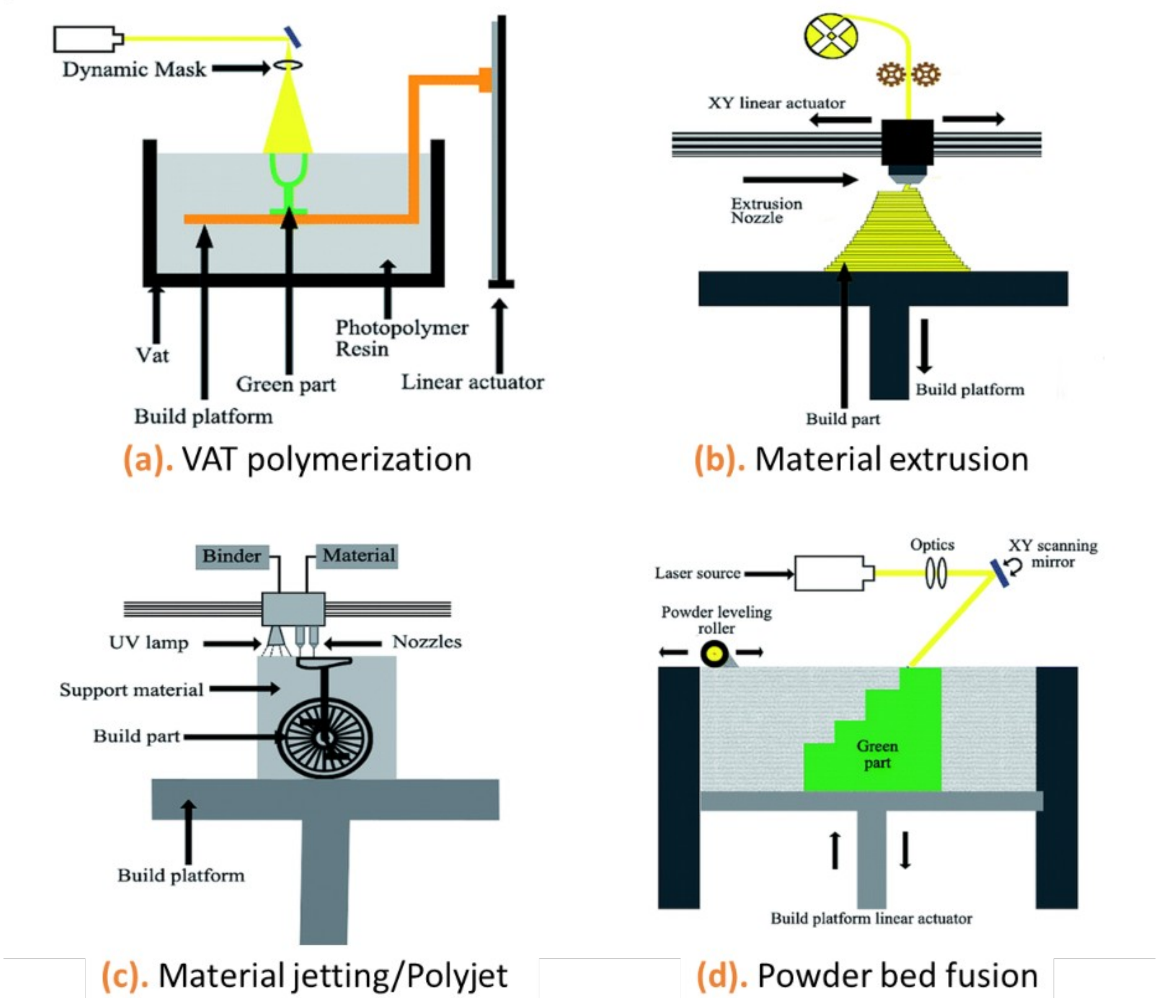

Figure 1. Schematics of 3D printing techniques used in feed spacer manufacturing. Reproduced from [66]. This figure is best viewed in color.

3.2. Critical Analysis of Spacer Manufacturing Methods

3.2.1. Key Manufacturing Metrics

Most 3D printing methods offer higher resolution, accuracy and precision than conventional extrusion, although they are inferior in printing speed and operational cost. We define these metrics below and compare them between manufacturing techniques in Table 4. This assessment of metrics is provided prior to the literature review, so that terminology and comparisons between the technologies can be better described when evaluating the literature.

3.2.1.1. Resolution

Resolution is defined as the minimum feature size that can be clearly depicted on the product. In spacer manufacturing, controlling spacer thickness, which determines channel height, is dependent on vertical (z-direction) resolution. Most spacers can have thicknesses ranging from hundreds of microns to several millimeters [23], and thus, have modest resolution requirements (unless elaborate surface features are required) enabling many 3D printing methods to be employed. Controlling spacer and filament thickness enables tuning CP, pressure drop [67] and foulant accumulation and localization in spacer grid [68].

Traditional extrusion (excluding FDM, an extrusion based 3D printing) is able to provide resolution below 100 μm [69]. However, the nature of conventional extrusion relies on dies and restricts the ability to precisely build filaments with different dimensional or morphological requirements (without making a new dye for each set of dimensions). Conventional extrusion is able to form a few shapes such as rods and films. However, conventionally fabricated spacers have low horizontal resolution as they are welded with extruded filaments. Although previous studies indicate the possibility to control porosity of extruded products [70], it is difficult for most extrusion techniques to form complex pore structures or geometries within filament layers.

3D printing techniques enable the formation of far more complex structures. The complexity of these structures is limited by the resolution. However, based on the resolution level of various 3D printing methods and spacer feature size range reported in our previous review paper [65], the resolution requirement due to feature size could be met by at least one or more 3D printing techniques. The feature size of the feed spacer discussed here refers to the minimum of spacer grid size or the thickness of the spacer filament.

3.2.1.2. Accuracy

Accuracy is defined as the structural deviation between the manufactured part and the model. Accuracy is an important factor in spacer manufacturing since the flow conditions in membrane modules are always predicted by models. Therefore, it is particularly important for a manufacturing method to make materials that could accurately represent the dimensions interpreted in the model. In spacer manufacturing, dimensional accuracy is particularly important as many feed spacers are manufactured based on CFD models, where closeness of spacer configuration to the simulated structure plays a key role in its performance. Die swell often occurs in polymer extrusion, in which the polymer is compressed to enter the die and partially expands and recovers to its original shape after leaving the die due to the viscoelasticity of polymer chains [71]. Therefore, the diameter of the extruded filaments is always larger than the die size, and the swelling ratio depends on both polymer physical properties (e.g., density, viscosity and molecular weight distribution) [72] and extrusion conditions (e.g., die geometry, shear stress, shear rate and temperature) [73]. As reported by Anand et al. [74], the swelling ratio of PP extrudate is at least 1.4, which makes it difficult to maintain unique size for each extruded filament for accuracy perspective. As reported by Tang et al. [75], there are theoretical models that predict the swelling ratio, which could be impacted by extrusion processing parameters (shear rate and temperature), die geometry, characteristics of polymer (molecular weight distribution) and filler. In terms of accuracy concern in 3D printing, Tan et al. [76] demonstrated that material jetting (PJT) showed less deviation in spacer structural parameters than powder-based or extrusion-based printing techniques, as illustrated in Figure 2.

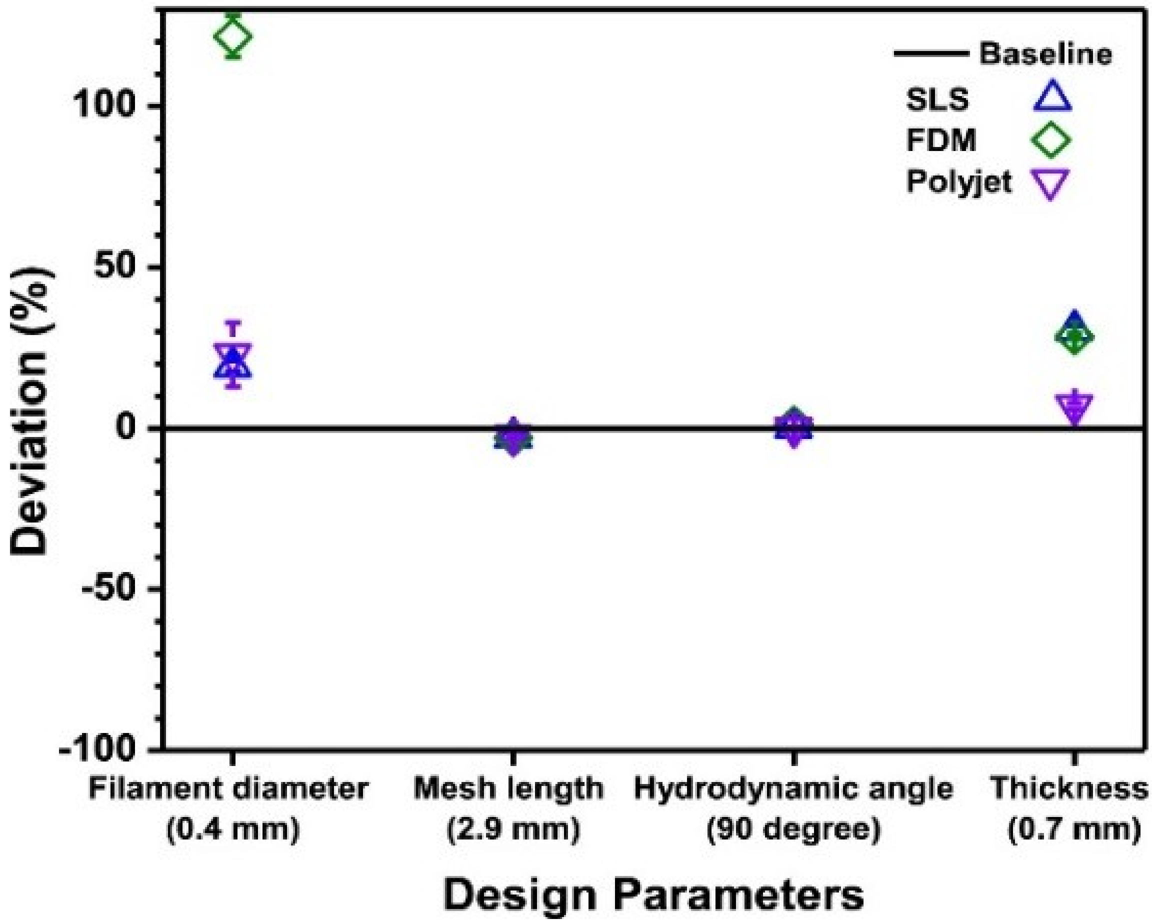

Figure 2. Deviation on spacer structural parameters for SLS, FDM and PJT [76]. This figure is best viewed in color.

3.2.1.3. Precision

Precision is defined as the structural difference between individually manufactured parts. Precision is an equally important metric in spacer fabrication as repeatability is a must for producing spacers with similar performance in SWE. When assessing the precision, tolerance is usually considered as an important standard to represent acceptable dimensional variation between printed products. The tolerance of FDM and SLA is around ±0.15%, and SLS could reach a precision level of ±0.3%. MJ has the highest tolerance level at ±0.1%, indicating its precise manufacturing efficiency.

Conventional extrusion provides a relatively decent precision, as the deviation in spacer filament thickness was reported to be less than 2% in a commercial net-type spacer [46].

3.2.1.4. Manufacturing Speed

Extrusion is a continuous process that enables rapid spacer formation in a roll-to-roll process. 3D printing is inherently batch, making its production speed substantially lower. On the other hand, most 3D printing methods need to achieve high quality in order to maintain details. Advances in 3D printing have increased process speed. For example, increasing the travel speed of the printer's nozzle could save significant amount of printing time. When printing thicker filaments, using bigger nozzle or print head could deposit greater quantities of materials. Printing a thicker layer with fewer number of prints could also yield the same product with reduced printing time. Maintaining a high temperature in the nozzle could enable "smooth printing" and avoid issues such as filament grinding due to incomplete melting of the filament [77].

3.2.1.5. Manufacturing Size

The size of the spacer is an important commercial viability metric as it could directly impact the scalability of membrane modules. In terms of manufacturing size, it is important to consider whether forming a large-scale spacer is appropriate for a certain technique. The width of feed spacers is usually relevant to the length of the membrane module. These elements can be between several to 40 m^2 [10,78] in an industrial-scale membrane module. The spacer size is usually relevant to the scale of the print bed. Many spacers with 1 m width and 0.5-0.7 m length could be easily printed out for an industrial-scale 8040 SWE. However, manufacturing size could restrict many 3D printing techniques to make spacers for larger scale modules that requires over 20m^2 area. Extrusion is good at manufacturing large-scale filaments as there is little size limitation on the length of the extruded filaments. Therefore, when welding these filaments together, the width of the spacer structure is also unrestricted. However, many modules are much smaller with the smallest typically being 1.8 inches in diameter and 12 inches long. Therefore, most 3D printing techniques, such as PBF, VP, FDM, have expanded their printing dimensions rapidly over the past few decades.

3.2.1.6. Cost

Membrane sheet and spacers are two major costs in membrane module, and both depend largely on their materials of construction. For example, PVDF and PES UF membranes and polyamide RO SWEs sell for about \$10-20/m^2 [79,80]. Based on a price quotation from Delstar in 2018, 31 mil mesh spacer costs \$0.35/linear ft and 80 mil rib spacer costs \$1.3/linear ft. Wholesale membrane prices, which can run \$4-6/m^2 for RO flat sheet membrane [81], are likely to drive the cost of a membrane module. While exact market pricing and a breakdown of module costs based on component is not publicly available, the spacer cost should not exceed the membrane cost for a module. This is a substantial limitation of 3D printed spacers. While cost data is not available for these newly developed spacers, they are likely to be far more expensive than conventional spacers in the near term.

In terms of module cost, a BW-4040 RO module could cost as little as \$240 at \$30/m^2. An SW30-8040 RO module could cost as little as \$390 at \$14/m^2. An TW30-2540 RO module could cost as little as \$170 at \$63/m^2 and a TW30-1812 RO module only costs \$27 at \$84/m^2. Expensive 3D printed spacers will raise the overall cost of membrane module. Therefore, whether it is worthwhile to reduce the pressure drop or fouling to a certain level for in increased module cost remains a question.

3.2.1.7. Structural strength

Spacer filaments must be elastic enough to be rolled or placed into a module without breakage or fraying. The flexural modulus of PP, for example, is approximately 1.5 GPa and its flexural strength is around 40 MPa [82], which indicates that PP is an easily bendable polymer, but also vulnerable to breakage under high stress. Compared with net-type spacers made of PP, most 3D printed spacers with other materials show better flexural performance. Some examples include [76]:

1. The ABSplus™ used for FDM printed spacers has a flexural strength of 65-75 MPa and flexural modulus of 1.7-2.2 GPa [83].
2. The EOS PA2200 for SLS printed spacers has a flexural modulus of 1.5 GPa [84].

3. The acrylic based monomer (VeroClear RGD810) used for PJT printed spacers has a flexural modulus of 2.2-3.2 GPa and a flexural strength of 75-110 MPa [85].

In addition to mechanical properties, it is also important to control the spacer porosity as higher porosity always leads to lower strength. Strength could also be reduced by internal defects, surface fracture or material anisotropy. Extrusion and subsequent welding may generate some structural inhomogeneities and defects in the spacer filaments. For example, under many circumstances, defects such as weld lines or internal pores are commonly observed during welding. While extruding polypropylene and polyethylene, melt fracture occurs as helical distortion on the filaments when they exit the die at a high speed. Therefore, maximum extrusion speed for most thermoplastic materials is usually below 750 rpm [86] to maintain mechanical strength of the filament. The mechanical anisotropy frequently observed in FDM printed parts is generally at the level of 50%, which could increase the uncertainty of mechanical vulnerability and potentially damage the spacer strength.

3.2.1.8. Surface Finish

A smooth surface finish on feed spacers is important since sharp-edged or rough surfaces could damage the membrane surface. In conventional extrusion, a rough surface is generally due to flow instability problems such as melt fracture and sharkskin [87], which typically result from high shear stress applied on the polymer and the loss of adhesion between polymer and extruder wall [88,89]. According to the roughness measurement conducted by Tan et al. [76], spacer surface with average roughness (Ra) values below 20 nm is considered smooth while Ra values higher than 100 nm are considered rough. Products printed by photopolymerization techniques such as SLA, DLP and PJT usually have smooth surface finishes due to the nature of crosslinked epoxy materials. Parts printed by SLS exhibit relatively rough or even porous surfaces due to the powder melting and sintering process.

3.2.1.9. Environmental and Safety Metrics

The manufacturing of polymeric feed spacers will inevitably generate hazardous chemicals, including ultrafine particles (UFPs, particles less than 100 nm) and volatile organic compounds (VOCs). The extrusion of PP could emit organic compounds such as pentane, propane and butane [90]. Compared with most 3D printing process, extrusion typically has high production rate that requires large amount of PP pellets to be fed at the same time. Since most hot-melt extruders have degassing screws to release residual volatile vapors, oligomers or decomposed materials, use of large quantities of organic compounds could impose safety and health risks for employees and nearby environment. The subsequent welding of spacer filaments has been reported to generate a range of other airborne contaminants [91].

Most 3D printing processes also generate a variety of hazardous chemicals. Studies have shown that the FDM printing of ABS filaments could release UFPs [92] and VOCs (mainly styrene) [93]. In SLS, during the powder delivery and sintering step it is easy for the operator to breathe in some powder dissipating in air. In VP processes, since large amounts of organic solvents are used for dissolving the resin, these volatile solvents could not only result in health risk, but also yield large quantity of toxic organic waste. During spiral wound module filtration, leaching of chemicals, especially surface coating from spacer into water could potentially release hazardous materials into the concentrate stream. Therefore, manufacturing safety infrastructure (i.e., ventilation, solvent capture systems, etc.), careful handling of chemicals, use of green solvents, and use of materials with reduced leaching are particularly important for the purpose of reducing health and environmental risks.

Table 4. Comparison on key metrics between 3D printing techniques and conventional extrusion

3D printing technique	Resolution	Accuracy	Material	Thickness per layer	Manufacturing speed	Manufacturing size	Reference
Conventional extrusion	sub-100µm	Dimensional tolerance of less than ±2% Die swell ratio of PP at least 1.4	Thermoplastics, metal, ceramic	N/A	Up to 750rpm for thermoplastics	No size limit	[Grida, 2003], [Liang, 2008], [Haidari, 2018]
SLS	70–100µm	Dimensional tolerance of ±0.3% Lower limit of ±0.3mm	Thermoplastics (Nylon), metal and ceramic powders	EOS GmbH: 0.06-0.15mm	EOS GmbH: 20mm/hr Up to 60mm/hr	Up to 750 x 550 x 550 mm	[Low, 2017], [Deckard, 1997]
SLA	Formlabs: 25-300µm Protolabs: X/Y: 200dpi	Dimensional tolerance of ±0.15% Lower limit of	Photopolymers	0.025mm-0.1mm Protolabs: 0.05mm	20-36mm/hr	Up to 1500 x 750 x 500 mm (industrial)	[Hull, 1984], [Low, 2017]

	Z: 62.5dpi 3D Systems: 50µm	±0.01mm					
DLP	Formlabs: X/Y: 35-100µm (depends on projector) Z: 25-300µm	Forecast 3D: ±0.05mm	Photopolymers	0.025mm-0.1mm	20-36mm/hr	192 x 120 x 230 mm	[Low, 2017]
FDM	10-300µm	Dimensional tolerance of ±0.15% Lower limit of ±0.2mm	Thermoplastics, polymer-based composites, ceramic slurries and clays, metal powders	Stratasys: 0.17mm - 0.33mm Ultimaker: 0.1mm-0.33mm	50-150mm/hr	Up to 1000 x 1000 x 1000 mm (industrial)	[Crump, 1992], [Low, 2017]
PJT/MJT	Stratasys: Z: 27µm Protolabs: XY: 305µm Z: 30µm	Stratasys: 14-600µm	Photopolymers	Stratasys: 14-28µm	17mm/hr	490 x 391 x 200 mm	[Stratasys, 2015]

3.2.1.10. Technology Readiness Levels (TRL)

As defined by NASA [94], the TRL represents a range of levels (0-9) that estimates the commercial maturity of technologies. This standard identifies level 0 indicates that a technology is entirely conceptional, while level 9 indicates the technology is fully commercial and proven. Based on this definition, conventional extrusion for spacers could be classified as level 9. Lezama-Nicolás et al. [95] reported the TRL of most 3D printing techniques, such as those reportedly used for spacer prototyping (PBF, ME, MJ, VP) fall in the range of level 6 to 7. The actual use of these techniques for spacer manufacturing are somewhat lower (Level 3-6). This does make comparison a bit difficult because some 3D printing techniques are not fully commercial as of yet.

3.2.2. Assessment of Manufacturing Techniques by Quantification of Key Metrics

In order to assess the overall spacer performance and commercial viability of the conventional extrusion and 3D printing techniques, we ranked each manufacturing method based on the aforementioned metrics in the range of 0 to 5. Resolution, accuracy, precision, structural integrity and surface finish were classified into spacer manufacturing benefits in actual spacer applications while fouling/scaling, CP, pressure drop and cleanability were considered as performance benefits in scientific publications. According to Pratofiorito et al. [96], spacer fouling was quantified by the fouling layer thickness (μm) per unit width of the spacer filament operated under 25 bar and 0.2ms^{-1} crossflow velocity. As indicated by previous literature [97,98], CP in spacer-filled channels could be quantified with CP modulus, as defined in equation (1).

$$M = \frac{c_m - c_p}{c_b - c_p} \quad (1)$$

Here c_m is the concentration on membrane surface, c_b is the bulk solution concentration and c_p is the permeate concentration. The pressure drop is quantified by normalizing the pressure drop with spacer length (or pressure gradient, kPa/m)[98]. The commercial viability metrics included cost, TRL, printing speed, size and environmental and safety. Levels of each metric are defined in Table 5. Assessment of all the manufacturing techniques in terms of key metrics levels were summarized in Table 6.

Table 5. Definition of each level of the metrics

Level	**0**	**1**	**2**	**3**	**4**	**5**
Resolution	Unable to control dimension at all	Able to form basic structures, such as pores (lower than 1 mm)	Lower than 80 μm	30-80 μm	Able to form smooth surface and sub-30 micron scale features	Able to form nanometer scale features
Accuracy	Unable to reach designed shape at all	Able to form general shape of the design, dimensional deviation larger than 50%	Dimensional deviation between 20%-50%	Dimensional deviation between 2%-20%	Dimensional deviation between 0.5%-2%	Dimensional deviation under 0.5%
Precision	Unable to form similar shapes	Able to form a certain shape, but with different dimensions	Able to form similar shapes with dimensional variation between 2-10%	Dimensional variation between 0.5-2%	Dimensional variation between 0.2%-0.5%	Dimensional variation under 0.2%
Structural integrity	Unable to form intact structure	Able to form structure, but deforms after manufacturing	More than 50% lower modulus or strength than parts made by the same material	5-20% lower modulus or strength than parts made by the same material	Similar modulus or strength as parts made by the same material	Higher modulus or strength as parts made by the same material
Surface finish	Roughness largely affects shape	Basic shape formed, but roughness at mm level	Roughness at micron level	Roughness between 100 nm-1 μm	Roughness between 10-100 nm. Could see roughness under microscope	Roughness below 10 nm
Fouling/	Fouling	Fouling	Fouling	Fouling	Fouling	Fouling

scaling control	layer thicker than 100 µm	layer 50-100 µm	layer 20-50 µm	layer 10-20 µm	layer 5-10 µm	layer thinner than 5 µm
Concentration polarization	CP modulus higher than 2	CP modulus 1.5-2	CP modulus 1.3-1.5	CP modulus 1.1-1.3	CP modulus 1.05-1.1	CP modulus below 1.05
Pressure drop	Pressure gradient higher than 100	Pressure gradient 80-100	Pressure gradient 60-80	Pressure gradient 30-60	Pressure gradient 10-30	Pressure gradient below 10
Cleanability	Irreversible and irrecoverable fouling	Irreversible fouling. Could be cleaned by chemical cleaning	Irreversible & reversible fouling, irreversible-dominant. Cleaned by long-term physical cleaning	Reversible dominant fouling. Cleaned by physical cleaning	Foulants only on the surface. Minor physical cleaning	No need to clean at all
Cost	Over \$100/m^2	\$60/m^2-\$100/m^2	\$30/m^2-\$60/m^2	\$10/m^2-\$30/m^2	\$5/m^2-\$10/m^2	Under \$5/m^2
TRL	0-2	2-3	3-5	5-7	7-8	9
Printing speed	Under 1 cm/hr	1 cm/hr-2 cm/hr	2 cm/hr-6 cm/hr	6 cm/hr-10 cm/hr	10 cm/hr - 1 m/hr	Above 1 m/hr
Size	Under 10 cm^2	10 cm^2 -100 cm^2	100 cm^2 - 500 cm^2	500 cm^2 - 1000 cm^2	1000 cm^2 -2 m^2	Above 2 m^2
Environmental and safety	Large amount of unrecyclable hazardous waste, UFPs and VOCs. Unsafe to operate with PPE.	Some unrecyclable hazardous waste, UFPs and VOCs. Safe to operate with PPE.	Reduced amount of recyclable waste, UFPs and VOCs. But needs PPE and takes long time to clean the machine.	Minor amount of recyclable waste, UFPs and VOCs. Needs PPE and cleaning after operation.	Trace amount of recyclable waste. Needs to wipe the machine after operation.	No waste and hazardous chemicals produced at all.

Table 6. Key metrics of each manufacturing techniques in terms of (a). manufacturing benefits and (b). performance benefits and (c). commercial viability of each manufacturing method.

Manufacturing technique	**Resolution**	**Accuracy**	**Precision**	**Structural integrity**	**Surface finish**	**Manufacturing benefits**	**Relative manufacturing benefits**

Conventional extrusion + welding	2	2	3	2	3	12	0
SLS	3	5	4	4	4	20	0.6667
SLS (15 years ago)*	3	4	4	3	3	17	0.4167
SLA	4	5	5	5	5	24	1
DLP	4	5	5	5	5	24	1
FDM	4	5	5	4	5	23	0.9167
PJT/MJT	4	5	5	5	4	23	0.9167

(a

Manufacturing technique	Fouling/ scaling control	Concentration polarization	Pressure drop	Cleanability	Performance benefits	Relative performance benefits
Conventional extrusion + welding	2	2	3	3	10	0
SLS	4	4	4	4	16	0.6
SLS (15 years ago)*	3	3	4	3	13	0.3
SLA	4	4	3	4	15	0.5
DLP	4	4	3	4	15	0.5
FDM	4	5	2	4	15	0.5
PJT/MJT	4	3	3	4	14	0.4

(b

Manufacturing technique	Cost	TRL	Speed	Size	Environmental and safety	Commercial viability	Relative commercial viability
Conventional extrusion + welding	5	5	5	5	2	22	1
SLS	3	3	2	4	2	14	0.6364
SLS (15 years ago)*	2	2	2	3	2	11	0.5

SLA	2	3	2	4	2	13	0.5909
DLP	2	3	2	3	2	12	0.5455
FDM	2	3	4	4	2	15	0.6818
PJT/MJT **(c**	2	3	1	4	2	12	0.5455

Note: This is a snapshot in time and will change over time.
* The benefits and commercial viability were evaluated based on the SLS spacers printed by Li et al. [44] and Blaster et al. [99].

A single quadrant chart displaying spacer performance and manufacturing benefits against commercial viability for all manufacturing techniques was shown in Figure 3. Conventional extrusion is far more viable than the 3D printing techniques, but it exhibits less ability to build complex spacer structures. We also recognize that this chart is a snapshot of time and the benefits and commercial viability of all 3D printing methods are expected to improve in the future, as demonstrated by the progress in SLS. There are some other non-quantifiable metrics, such as logistics, and material availability, that may depend on location.

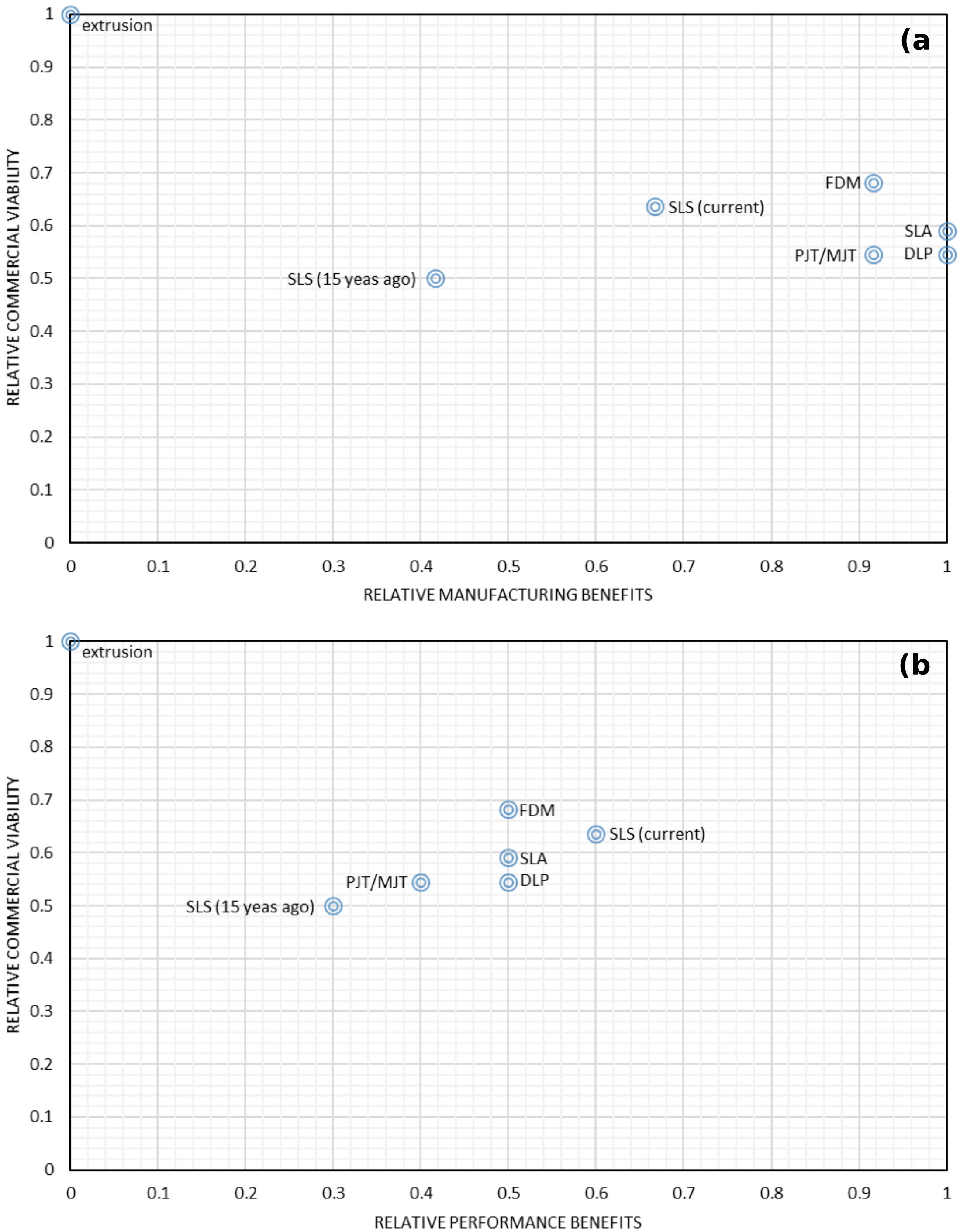

Figure 3. 4-quadrant chart showing relative commercial viability versus relative manufacturing (a) and performance benefits (b) and of different spacer manufacturing techniques. Relative values were calculated based on the benefits and commercial viability of conventional extrusion set at (0,1). This figure is best viewed in color.

4. 3D Printed Spacers

This section will summarize recent studies on using a variety of 3D printing techniques in printing functional feed spacers for various membrane applications. Table 7 summarizes the application, geometry, material and printing method of various 3D printed feed channel spacers reported in recently published papers.

Table 7. Application, material, printing technique and geometry of various 3D printed feed channel spacers.

Application	Spacer geometry	Material	Printing technique	Remarks	Reference
Membrane separation	Modified filaments, twisted tapes, multilayer spacers	N/A	SLS	The optimal multi-layer spacer showed 30% higher Sherwood number and only 40% of the power consumption compared with optimal non-woven spacer.	[Li, 2005], [Li, 2003]
Electrodialysis desalination	Single and multilayer spacers with various filament geometries	N/A	SLS	Single layer spacer with 60˚ rectangular twisted filament had the highest mass transfer. Hybrid multi-layer spacer had 20% higher mass transfer than standard non-woven spacers.	[Balster, 2006]
RO, UF	TPMS	Polyamide 2202	SLS	The incorporation of TPMS spacers enhanced flux, reduced biofouling and pressure drop.	[Sreedhar, 2018]
MD	TPMS	Polyamide 2202	SLS	3D printing different TPMS spacers to control scaling in MD.	[Thomas, 2019]
MD	TPMS	Polyamide 2202	SLS	The best TPMS spacers had 60% higher water flux and 63% higher heat transfer coefficient.	[Thomas, 2018]
MD	TPMS	Polyamide 2202	SLS	The 3D Gyroid spacer showed improved flux, 85% water recovery and the best organic fouling mitigation capacity.	[Castillo, 2019]
MD	TPMS	Polyamide	SLS	There was a marginal flux	[Thomas,

		2202		improvement (up to 17%) by installing the Schwartz P style TPMS spacer in AGMD. However, a pronounced pressure drop decrease of 50% was achieved.	2021]
UF	TPMS	Polyamide 2202	SLS	Thicker tCLP-TPMS spacers still exhibited 16.67% lower fouling resistance and 13.33% lower membrane cleaning resistance than the thinner net spacers.	[Sreedhar, 2020]
Wastewater treatment	Net-type	PP	SLS	Higher printing energy induced stronger mechanical properties but lower accuracy of spacers.	[Tan, 2016]
NF	Honeycomb-shaped hexagonal	Nylon powder	SLS	A thinner fouling layer with higher turbulent kinetic energy was formed on the hexagonal spacer, which achieved a flux increase of 26.4%.	[Park, 2021]
MF	Hill like, wavy, perforated	Polyamide	SLS	The wavy spacer with perpendicular flow direction enabled higher turbulence kinetic energy and surface shear rate than the hill-like spacers. At high permeate fluxes (40 and 60 LMH) the spacer perforated with small holes (1 mm) exhibited 25% lower fouling rate than non-perforated spacers.	[Tan, 2019]
Wastewater treatment	Net-type	Polyamide-12 (PA 2200)	SLS, FDM, Polyjet	All 3D printed spacers showed higher mass transfer than commercial spacers. Compared the impact of 3D printing technique on membrane performance and fouling.	[Tan, 2017]
RO, UF	Ladders, herringbones, helices	ABS	FDM	High mass transfer coefficients observed on all three types of 3D printed spacers.	[Shrivastava, 2008]
FO	Diamond-shaped	ABS, PP and PLA	FDM, Polyjet	Compared impact of AM technique and material on printing precision, mechanical properties, filtration performance and fouling resistance of spacers.	[Yanar, 2018]
FO	Diamond-shaped, hexagonal	PP	Polyjet	The hexagonal spacers could reduce reverse solute flux by 50%, improve flux and	[Yanar, 2020]

				antifouling performance.	
RO, NF	Diamond-shaped spacers with modified filament angle and mesh size	Urethane acrylate polymer	Polyjet	Both numerical modelling and MFS studies indicated 3D printed spacers had lower pressure drop and low biofouling impact on performance.	[Siddiqui, 2016]
UF	Double-helix form twisted filament	N/A	Polyjet	The novel spacers showed enhanced mass transfer and selectivity in crossflow condition.	[Fritzmann, 2014]
UF	Net spacers with 1,2,3 helices along the filament	Acrylate monomer, BV-007	DLP	3-helical spacers showed lower pressure drop, higher average specific flux and best fouling mitigation performance.	[Kerdi, 2020]
Submerged membrane filtration systems	Double-helix form twisted filament	N/A	Polyjet	The novel spacers showed improved flux, reduced aeration rate and higher antifouling efficiency.	[Fritzmann, 2013]
MF/UF	Herringbone, TPMS gyroid	Visijet M3 Crystal (UV curable plastic)	Multijet	The TPMS gyroid spacer showed 81% and 93% flux enhancement in blood and plasma mimicking solution tests and 23% higher pressure drop.	[Dang, 2021]
UF	Static mixing spacer design	N/A	SLA	The novel spacer design could help improve mass transfer and reduce pressure drop.	[Liu, 2013]
UF	1-hole, 2-hole and 3-hole perforated spacers	Liquid resin (acrylate monomer, BV-007)	DLP	1-hole spacer provided 75% flux enhancement and fouling reduction. 3-hole spacer provided 54% less pressure drop at the cost of smaller flux increase.	[Kerdi, 2018]
FO	Hole-type spacers	Liquid resin (acrylate monomer, BV-007)	DLP	Perforated spacer was found to increase the permeate flux slightly more than standard spacer. Perforated spacer exhibited severer flux decline and better pressure drop control than standard spacer.	[AlQattan, 2021]
UF	Spacers with cylindrical column type nodes	Liquid resin (acrylate monomer, BV-007)	DLP	The column spacers created wider clearance zone, which induced twice higher flux, two folds of energy consumption reduction and three times lower pressure drop compared with standard	[Ali, 2019]

				spacers.	
FO	Turbospacers composed with microturbines	acrylate monomer (BV-007)	DLP	The turbospacers showed approximately 15% lower flux decline, 2.5 times lower foulant resistance and 2 folds less pressure drop compared with standard spacers.	[Ali, 2021]
UF	Turbospacers composed with microturbines	acrylate monomer (BV-007)	DLP	The turbospacers showed 4 times lower pressure drop, over 3 times higher specific permeate flux and 2.5 folds lower specific energy consumption than standard spacer.	[Ali, 2020]

4.1. SLS Printed Spacers

The first 3D printed feed spacer was made and tested by Li et al. [44,100] via SLS. In this work, intricate geometries were embedded into 2 layers of nonwoven net spacer meshes to form a multi-layer spacer structure. The authors compared the mass transfer enhancement of these spacer structures experimentally and also concluded that CFD simulation of these complex spacers were unreliable due to their complex geometry. Additionally, the 3D printed multi-layer spacer comprising non-woven nets as outer layer and twisted structure as middle layer displayed 30% higher Sherwood number at the same power consumption level and 60% lower crossflow power consumption at the same mass transfer compared with optimal non-woven spacer. This is the earliest research that relied on 3D printed multi-layer spacers with experimentally confirmed higher mass transfer and lower power consumption, which avoids the dependence on CFD simulation when a novel spacer design is proposed.

Blaster et al. [99] investigated the mass transport behavior of both single and multi-layer SLS printed spacers to decrease CP in electrodialysis desalination. Single layer spacers were printed by Li et al. [44] via SLS and they were also assembled into multi-layer spacers for mass transport studies. The influence of spacer geometry, including the filament angle, shape and flow attack angle was studied for the purpose of optimizing the structure of single spacers. For single-layer spacers, due to the creation of swirling flows, the 3D printed spacer with filament angle of 60° in a rectangular twisted shape displayed the highest mass transfer. The multi-layer spacers combining middle spacer with round filaments and a flow attack angle of 45° with two thin net spacers on the outside, exhibited 40% higher enhancement in mass transfer than a 3D printed single spacer. However, the authors also found multi-layer spacers incorporating the same outer layers, but a commercial non-woven spacer as mid-layer showed the same mass transfer enhancement, but 30 times lower power consumption compared with the multi-layer spacer mentioned above. This study successfully tackled the problem of CP in electrodialysis by incorporating multi-layer spacers consisting various spacer assembly. However, it did not conduct the CFD simulation to model the flow pattern inside the multi-layer spacers, which is important in studying the impact of spacer geometry on mass transfer. It is also interesting to study whether these spacers could impact the ion transport or their impact on the boundary layer in electrodialysis.

Sreedhar et al. [46] designed novel spacers structures based on previously optimized TPMS mathematical architectures for the purpose of flux improvement and fouling mitigation in UF and RO processes. TPMS is a mathematically design surface developed by Schwarz [101,102] with minimal surface area at a given boundary. The TPMS spacers with various structures used in this research are shown in Figure 4. There is no self-intersection and any enfolded surface in its internal channels, which is beneficial for mass transfer and could help enhance the flow. The spacers with 3 different TPMS structures were printed via SLS converted from predesigned CAD files. The printed spacers were subsequently placed on the feed side of the commercial polyamide and polyethersulfone membranes. Control samples were made by incorporating commercial net spacer on the same membranes. The membranes with spacers printed in Gyroid structure exhibited an 15.5% and 38% higher flux than those used with a commercial spacer in brackish water RO and UF tests, respectively. In the biofouling test compared with commercial spacer, this spacer showed 91% reduction in cells attached to membrane surface. This work utilizes the ability of 3D printing to form a theoretically optimized structure and offers a great potential for a variety of TPMS structures in feed spacer applications. Thomas et al. [5] demonstrated the success of the TPMS spacers in tuning the flux-pressure drop tradeoff relation in membrane distillation by forming new spacers from the combination of tCLP and Gyroid TPMS structures. Since pristine tCLP spacer enhanced flux at the cost of tremendously increasing pressure drop, the authors formed the hybrid spacer with tCLP structure in the midsection and the Gyroid structure at the ends. The hybrid spacer exhibited similar flux enhancement with higher antifouling ability and 60% reduction in pressure drop compared with the tCLP spacer. In another work [45] the authors compared five novel TPMS spacers with commercial spacer in terms of water flux and heat transfer in direct contact membrane distillation (DCMD). They observed the tCLP spacer, with the highest surface area to volume ratio, induced highest turbulence and exhibited 60% higher water flux with 63% higher film heat transfer coefficient compared with the commercial spacer. In another study [47], the same research group demonstrated the 3D printed TPMS spacers only presented 17% flux improvement in air gap membrane distillation (AGMD). However, compared with commercial net spacer, a 50% lower pressure drop was observed by installing the Schwartz P style TPMS spacer in AGMD, which indicates the opportunity to simultaneously enhance flux and reduce the operating energy cost in an MD plant. Thomas et al. [103] compared the antiscaling performance of 3D printed polyamide TPMS (Gyr-tCLP hybrid) spacers coated by fluorinated silica (FS) and a variety of graphene oxide or graphene nanosheets. In the DCMD experiment it was found out that the FS surface coating resulted in the largest enhancement in antiscaling performance with a 74% and 60% reduced scalant attachment on the spacer and membrane, respectively. The minimized scaling was mainly attributed to the increased spacer surface roughness, which consequently led to higher hydrophobicity and reduced surface-free energy to weaken the scalant-spacer surface interaction. In another work [48] they compared the fouling and cleaning efficiency of commercial net-type PP spacers with 3D printed tCLP TPMS spacers. Although the tCLP spacers were printed with higher thickness of 2.3 mm, they still exhibited approximately 16.67% lower fouling resistance and 13.33% lower membrane cleaning resistance than the 1.2 mm net spacers. This result suggests that the spacer design could impact the shear stress in spacer-membrane contact area and consequently influence the membrane fouling and cleaning efficiency. In another paper Castillo et al. [104] studied the impact of the tCLP and Gyroid TPMS spacers on organic fouling mitigation in direct contact MD (DCMD). The authors found out both TPMS spacers could greatly enhance the permeate flux (up to 200%) compared with 30-70% flux enhancement by the commercial spacer. The 3D printed Gyroid spacer exhibited only 12% flux decline in organic fouling test and 85% water recovery, which was primarily attributed to the tortuous internal geometry of this Gyroid design that can repel the foulants.

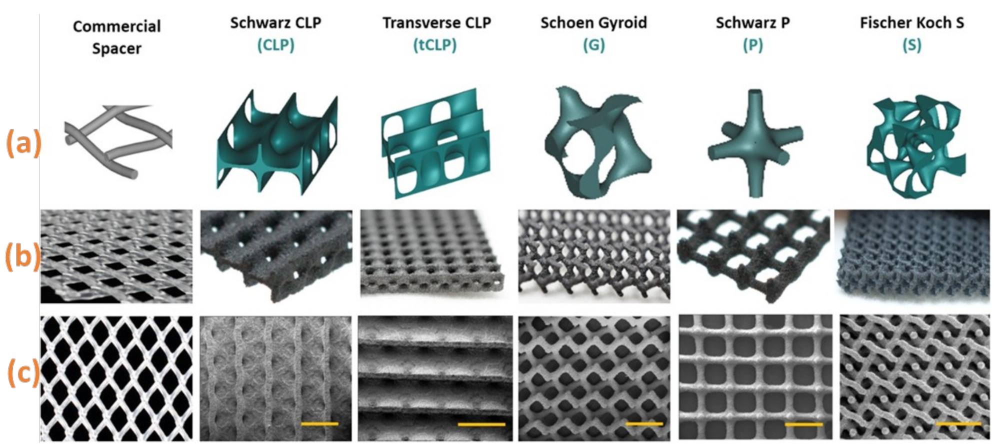

Figure 4. 3D printed TPMS feed spacers in different structures: (a) Volume element; (b) Photographs and (c) Top view SEM images. Reproduced from [45]. This figure is best viewed in color.

Tan et al. [105] investigated impact of printing conditions on the mechanical properties of SLS printed polypropylene (PP) net-type spacers. In order to avoid damages on both themselves and the membrane surfaces during the rolling-up process of the spiral wound module, spacers with high ultimate strength, considerable Young's modulus and small dimensional variation are preferred. Their work indicated that Young's modulus and ultimate strength of the printed net-type samples show a positive correlation with the printing energy density. However, when higher energy density was applied, larger dimensional variations appeared on both spacer height (40-100%) and filament diameter (100-300%). The structural inaccuracy will not only impact the mechanical properties, but also, spacer surface finish and their performance in the spiral wound module.

Park et al. [106] demonstrated SLS printed honeycomb-shaped hexagonal spacers (Figure 5(a)) could effectively mitigate fouling in NF spiral wound module. It is demonstrated in Figure 5(b) that compared with the SLS printed diamond-shaped standard spacers where a thick fouling layer of 175.5 μm was observed, the fouling layer formed on the hexagonal spacers structured as a unique mountain shape. This unique shape of the fouling layer also came with higher turbulent kinetic energy that reduced CP. Therefore, under high fouling conditions, the use of hexagonal spacers could achieve a flux increase of 26.4% compared with only 9% flux increase by installing the standard spacers, as illustrated in Figure 5(c).

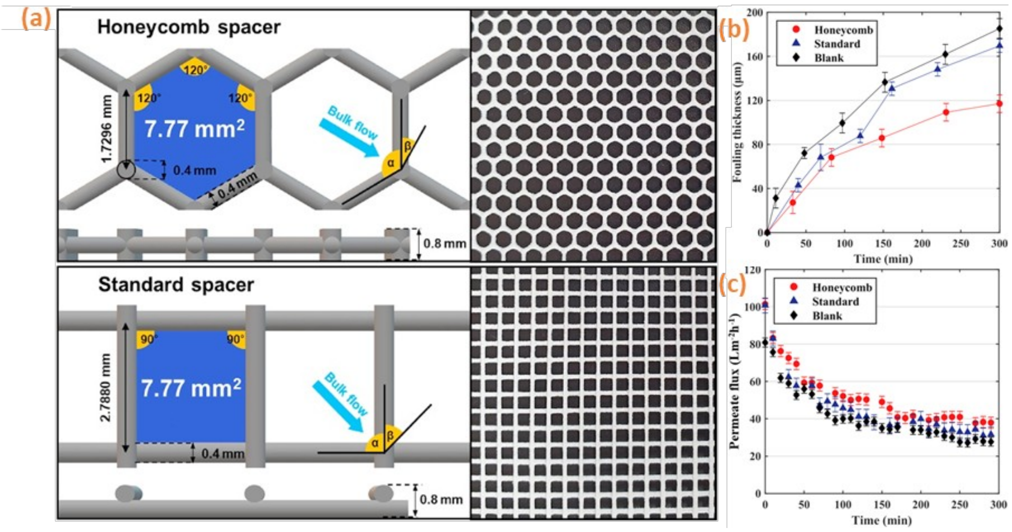

Figure 5. (a) 3D printed hexagonal honeycomb spacer and standard spacer. Comparison on (b) fouling layer thickness and (c) permeate flux of the spiral wound module with honeycomb-shaped spacer (red), standard spacer (blue), and empty feed channel (black) under high fouling conditions: ($CaCl_2$: 2 g/L; humic acid: 20 mgC/L; pressure: 20 bar; velocity: 0.35 m/s). Reproduced from [106]. This figure is best viewed in color.

Tan et al. [107] studied the fouling mitigation of various 3D printed vibrating spacers in a submerged flat-sheet membrane MF system. Hill-like spacer and wave-like spacers with different feed flow orientation and perforation sizes were printed by an SLS printer, as shown in Figure 6(a). The wavy spacer with perpendicular flow direction were superior to a hill-like spacer and awavy spacer with parallel flow direction as the perpendicular flow enabled higher turbulence kinetic energy and surface shear rate in the wavy structure. In terms of spacer perforation, perforated spacers did not show obvious enhancement at low permeate flux (20 LMH) with low fouling extent. However, at high permeate fluxes (40 and 60 LMH) the spacer perforated with small holes (1 mm) exhibited approximately 25% lower fouling rate than non-perforated spacers.

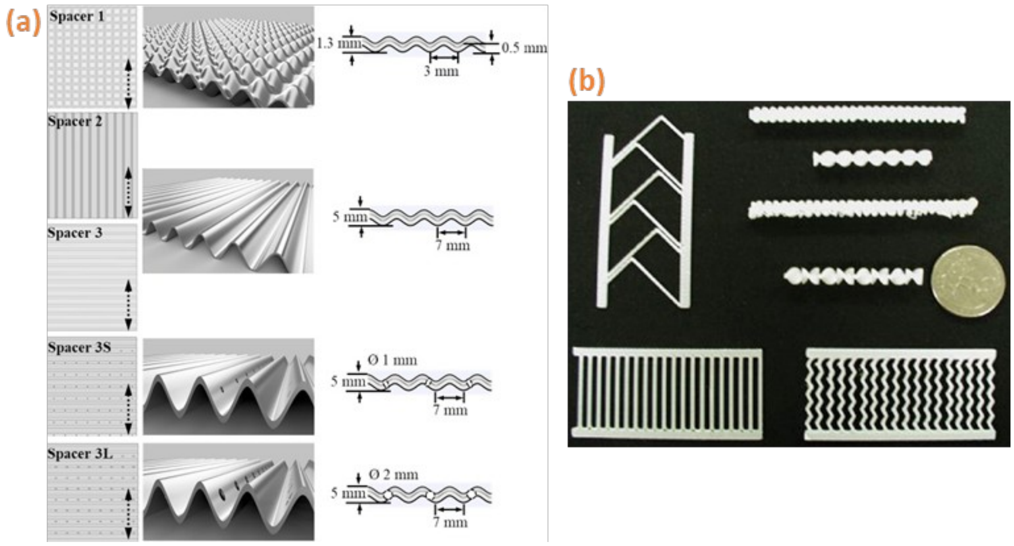

Figure 6. (a) Spacer 1: SLS printed hill-like spacer. Spacer 2, 3: SLS printed non-perforated wavy-like spacers with different orientation to feed flow. Spacer 3S, 3L: SLS printed feed spacers with 1 mm (spacer 3S) and 2 mm (spacer 3L) perforation. Reproduced from [107]. (b). FDM printed herringbone and helically shaped spacers. Reproduced from [108]. This figure is best viewed in color.

4.2. FDM Printed Spacers

Shrivastava et al. [108] printed ladder-shaped, herringbone-shaped and helically shaped spacers via FDM, as shown in Figure 6(b). The purpose of their work was to explore the effect of each spacer shape on CP in UF and RO processes and propose a reliable guide for designing better spacers. The authors demonstrated large mass transfer coefficients observed in their electrochemical measurements of mass transfer on all three types of spacers. The results of ladder-shaped spacer showed little derivation from the CFD simulation, but the herringbone and helical shaped spacers produced large discrepancies between the electrochemical measurements and their CFD simulation. This also brings a further question that the current measurements in electrochemical measurements may not be directly translated to UF and RO since they are flow processes rather than diffusion processes.

4.3. Polyjet/Multijet Printed Spacers

Yanar et al. [109] compared the mechanical properties, water flux, reverse solute flux and fouling behavior of 3D printed honeycomb spacers with commercial PP spacers in forward osmosis (FO). The PP spacers were printed by a Polyjet printer and the PLA and ABS spacers were printed by a FDM printer. The authors looked into the dimensional derivation of these spacers by comparing them to the thicknesses designed in the CAD files. The ABS spacer was found to have the worst precision with a 11.93% higher thickness (962.6 μm) due to its well-known swelling behavior. The PP spacer, with a thickness of 835.2 μm, also displayed some deviation due to material shrinkage during Polyjet printing. The PLA spacer showed only 0.34% width deviation and a thickness of 857.1 μm and it also showed the highest yield strength of 0.433 MPa. The PP, PLA and commercial spacers all showed strong elasticity during the tensile test, while the ABS spacer demonstrated plastic behavior. In terms of water and reverse solute flux, the ABS spacer was found to have higher water flux (2.52 gMH) and similar solute flux as the commercial spacer due to its smooth surface finish. Although PP and PLA spacers exhibited lower water flux than commercial and ABS spacers, they demonstrated much better membrane fouling performance. Recently the same group incorporated Polyjet printed PP spacers in flat sheet FO membranes to reduce membrane surface shear stress, which could assist in reduction of fouling and reverse solute flux [110]. The authors printed two hexagonal honeycomb spacers with vertical and horizontal orientation to compare their performance in FO. They found out the vertically oriented honeycomb spacers exhibited identical shear stress in all the three directions while the horizontally oriented spacer had uneven shear stress distribution on its filaments. Therefore, vertically oriented spacer exhibited 50% reverse solute flux reduction and 56% less foulant adhesion than horizontally oriented spacers. Their research indicates that selection of printing condition and spacer material are important in spacer performance as polymeric materials shrink or swell differently in various condition, which can result in different surface finish and dimensional accuracy. Their paper also suggested that in terms of spacer geometry, other than macroscopic shape, filament orientation also matters in membrane performance since it can directly affect the surface stress distribution.

Siddiqui et al. [111] compared the 3D printed mesh-like diamond shape feed spacers with conventional spacers based on the combined analysis of numerical modeling and experimental membrane fouling simulator (MFS) studies. One set of spacers were printed via Polyjet printing following the same geometry of conventional spacer. Another set was Polyjet printed with the same thickness but larger mesh-size and smaller filament angle. The hydrodynamic behavior of the spacers was numerically modeled by COMSOL and the fouling behavior was studied via a specific MFS setup. The conventional spacer and the 3D printed spacer with the same geometry displayed similar hydrodynamic and biofouling behavior based on the numerical modeling and MFS results. The 3D printed spacer with modified geometry displayed a 60% lower pressure drop at a specific flow rate in the hydrodynamic modeling and MFS test. MFS test also showed that at a fixed biomass accumulation the modified 3D printed spacers had 34% lower pressure drop, indicating lower impact of biofouling on the spacer. This study successfully demonstrated a precise way to form a desired geometry via Polyjet printing and proposed a numerical-experimental combined strategy in developing spacers in other applications such as FO and MD.

Fritzmann et al. [4] printed microstructured spacers (MSS) with twisted double-helix filament (Figure 7(a)) and compared it with commercial net spacers for the purpose of understanding the impact of spacer geometry on UF process. The spacers were printed via Objet rapid prototyping, a typical Polyjet technology and they comprised two layers of double-helix form filaments partially fit into each other in opposite twist orientation with 80% porosity. The 3D printed spacers exhibited improved mass transfer performance and a 50% higher flux than net spacers at the cost of higher pressure drop in crossflow condition, as shown in Figure 7(c). As indicated in Figure 7(c), the printed spacers showed flux between 70-180 LMH and pressure loss from 0-240 bar/m with 0-1 m/s flow rate. In Figure 7(b) the printed spacers show lower $MWCO_{90}$ than the net spacers. Since higher flux yielded stronger CP, the MWCO of dextran solution increased substantially for all spacers types. As a comparison, Kerdi et al. [112] printed net-type spacers composed of 1,2,3 helices along the filaments via DLP (79.5%, 79.4% and 79.1% porosity respectively). Increase in number of helices was found to enhance the flux and lower the pressure drop. The 3-helical spacer was found to have 640 LMH/bar average specific flux at 0.162 m/s flow rate and 430 LMH/bar average specific flux at 0.188 m/s flow rate. When the flow rate increased from 0.009 m/s to 0.304 m/s, the 3–helical spacer had pressure drop increased from 20.9 Pa/m – 63,615 Pa/m, which was lower than spacers with 1 or 2 helices. The OCT images also demonstrated that the 3-helical spacers perform the best (bio)fouling mitigation than spacers with fewer helices. In another paper, Fritzmann et al. demonstrated the use of these Polyjet printed MSS spacers in flat sheet submerged membrane bioreactors (MBR) and studied the reduction in air sparging, energy consumption and membrane fouling [113]. The helical shape in the filament could increase the shear force applied on membrane and create new path for the bubbles in the MBR, which was able to improve bubble cleaning efficiency. In critical flux measurements, the authors found a 100% flux increase by implementing the MSS spacers in the feed channel. The printed spacers could also reduce the aeration rate by 7.5 times at high crossflow velocities without influencing the other process performance. Based on this, they proposed that the best way to improve antifouling efficiency is by employing these MSS spacers at high crossflow velocity. These spacers also demonstrated possible potential in reducing energy consumption when placed in the side stream for fluids with higher solid loading. However, the authors did not study mechanical properties of the spacers especially the shear modulus since there might be deformation under high velocity crossflow condition. Also, the paper should also demonstrate the potential damage on membrane surface imposed by the sharp edge of the twist helical filament and also accuracy and precision requirements when printing these intricate spacer structures.

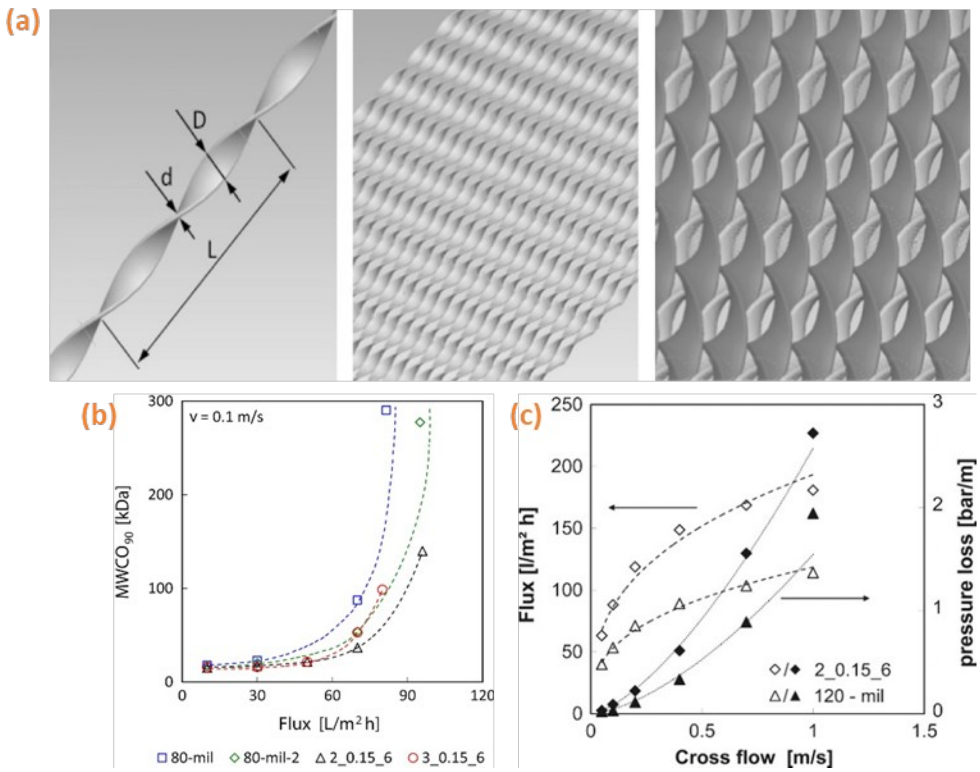

Figure 7. (a) PJT printed double-helix form twisted filament (left), single layer of twisted elements (middle), and two-layer spacer (right). Reproduced from [113]. (b) Comparison on helical and net spacers on molecular weight at 90% dextran rejection ($MWCO_{90}$) at 0.1 m/s. Feed solution contains a variety of dextran at different molecular weight. (c) Flux and pressure loss dependency on cross flow velocity for helical and net spacers. Reproduced from [4]. This figure is best viewed in color.

Dang et al. [114] compared the flux enhancement and pressure drop induced by herringbone spacers and the TPMS spacer in MF and UF narrow channels, as shown in Figure 8(b). Figure 8(a) shows the spacer structures with different feature sizes between 100-400 μm in both herringbone and TPMS Gyroid shapes printed by a multijet 3D printer. The TPMS spacer exhibited significantly higher flux enhancement than the herringbone spacers as it showed 81% and 93% flux enhancement in blood and plasma mimicking solution tests, although it also came with 23% higher pressure drop.

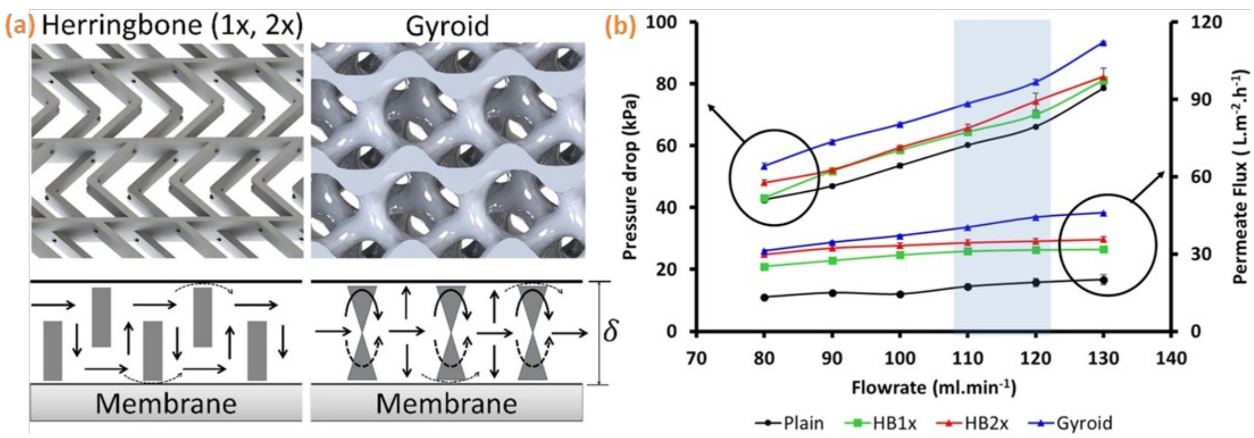

Figure 8. (a) CAD designs of herringbone spacers (top left), TPMS-Gyroid spacer (top right) and corresponding flow patterns in the feed channel (bottom). (b) Comparison on pressure drop and permeate flux at different flow rate in feed channel without spacer, with two types of herringbone spacers and TPMS-Gyroid spacer. Reproduced from [114]. This figure is best viewed in color.

In another paper, Tan et al. [76] compared the performance and accuracy of commercial feed spacers with polyamide spacers printed via SLS, FDM and Polyjet (Figure 9(a)). FDM printed spacers exhibited smoother surface, but lower accuracy than spacers printed by SLS and Polyjet. In terms of membrane performance, the SLS, FDM, Polyjet printed spacers showed higher mass transfer and flux than the commercial spacers, as indicated in the Sherwood number - Power number correlation in Figure 9(b). Spacers printed by FDM displayed the highest improvement in mass transfer and critical flux, which indicated their highest potential in fouling and CP reduction. Now, in addition to accuracy, surface finish is also important structural property that will impact spacer performance. As shown in Figure 9(a), (c), although FDM has the lowest accuracy it produces smooth surface, as reflected in its highest enhancement of mass transfer. This paper also suggests that there is always a tradeoff between mass transfer enhancement and pressure loss, and spacers printed by these techniques could not avoid such tradeoff.

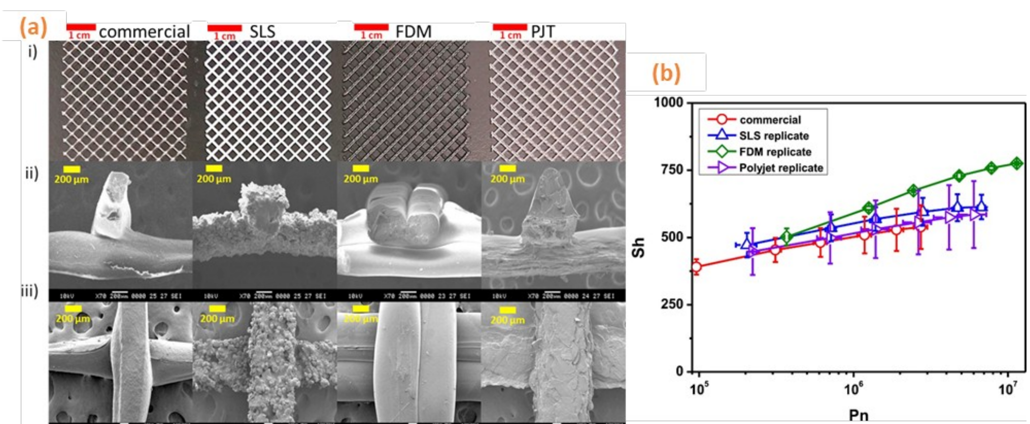

(c)

	Method			
Performance	Commercial	SLS	FDM	Polyjet
Accuracy of geometry	√√	√√√	√	√√√√
Pressure loss minimisation	√√√√	√√√	√	√√
Mass transfer enhancement	√	√√√	√√√√	√√
Critical flux enhancement	√	√√	√√√√	√√√
Bacteria attachment reduction	√√√√	√√	√√√	√

Note: √: Limited √√: Low √√√: Moderate √√√√: High.

Figure 9. (a) SLS, FDM, Polyjet printed and commercial net-type spacers, with front view and top view morphologies under SEM. (b) The Sherwood number - Power number relationship of all 4 types of spacers. (c) Comparison on geometrical accuracy and UF performance of all 4 types of spacers. Reproduced from [76]. This figure is best viewed in color.

4.4. SLA Printed Spacers

Liu et al. [115] proposed a specific design of static mixing spacer element, which was able to lead the fluid adjacent to the upper and lower membrane surfaces into a flow channel for the purpose of enhancing mixing of the flow, as demonstrated in Figure 10(a). Multiple spacer elements were assembled together to create flow path, allowing feed flow to be mixed well, as demonstrated by the flow streamlines in Figure 10(b). Compared with the regular feed spacer, which generated mixing usually by creating turbulence or fluid vortices at the cost of higher pressure drop and energy consumption, this static mixing spacer was able to mix the fluid flowing through the top and bottom boundaries. Based on the Sherwood number - Power number correlation, this novel spacer displayed similar mass transfer coefficient at high power inputs and a 20% higher mass transfer at low power inputs compared with the conventional spacer (Figure 10(d)). The authors also found lower wall concentration for the static mixing spacers compared with diamond spacers (Figure 10(c)), suggesting better mass transfer. However, this spacer design is still limited for membrane processes as its feed channel pressure drop is even higher than the conventional spacers. Additionally, the authors did not mention whether the sharp edge of the spacer could damage the membrane surface. The accuracy and surface finish of the spacer were also not studied as they could impact the fluid mixing and boundary layer flow in spiral wound module.

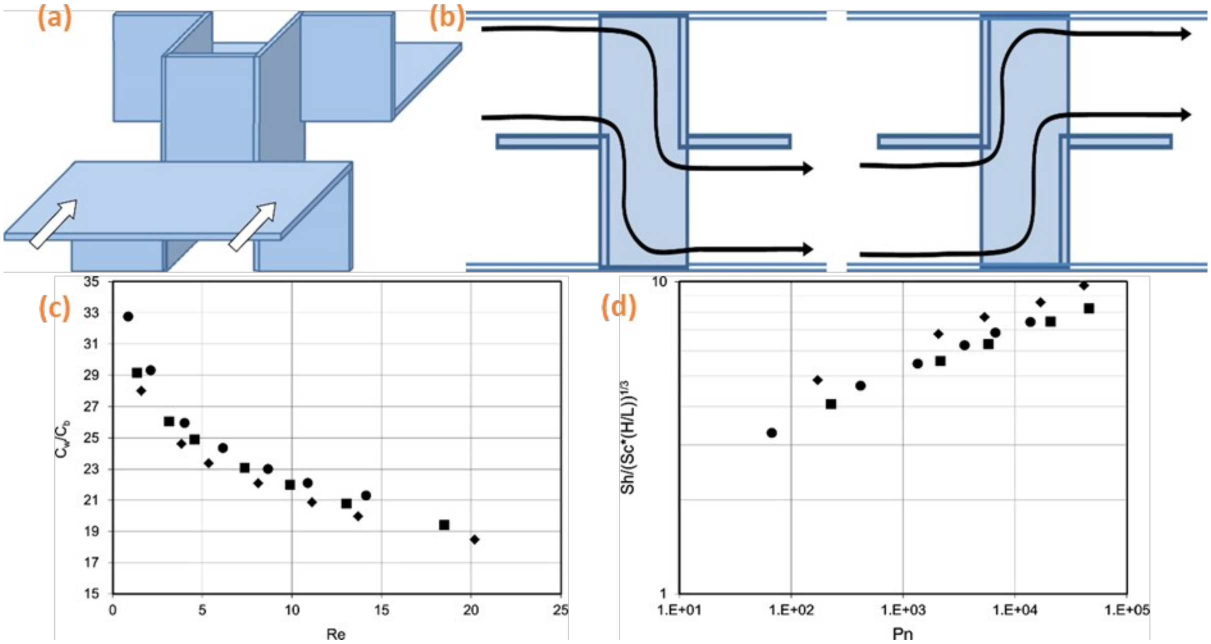

Figure 10. (a) Static mixing spacer design. Flow direction is defined by the arrow. (b) Streamlines of flow in the static mixing spacer (cross section view). (c) Concentration polarization modulus as a function of Re for different spacers. (d) Scaled Sherwood number as a function of Power number for different spacers. Circle—conventional spacer; diamond— 13 equally spaced spacer 1 elements, square—13 equally spaced spacer 2 elements. Feed pressure: 120 kPa; dextran concentration: 5.0 kg/m^3. Reproduced from [115]. This figure is best viewed in color.

4.5. DLP Printed Spacers

Kerdi et al. [116] proposed a series of perforated spacers, which can be printed precisely with a commercial DLP printer with a resolution of 25 μm. Spacers perforated with one, two, three holes were printed and compared with the standard spacer without perforation (Figure 11(a)). The spacers were placed on the feed side of a commercial UF membrane and tested in a crossflow system under two sets of experiment conditions: constant feed pressure at 60 kPa or constant feed flow rate at 12 L/hr. In both case it was found that all the perforated spacers displayed a higher flux, lower pressure drop and reduction in fouling compared with the unperforated spacer. As demonstrated in Figure 11(b) and (c), under constant feed pressure, the 1 hole perforated spacer demonstrated the best flux performance by an increase of 75% and a small reduction in pressure drop of 15%. The 3-hole spacer showed a much better efficiency in reduction of pressure drop (54%) at the cost of a lower improvement in flux (17%). The authors also studied the flow pattern between the perforated filaments and found out that the micro-jets passing through the filaments were able to fill the dead zones thus improving the flux. The turbulent jet within the spacer could also generate membrane cleaning and reduce fouling. The CFD simulation on the micro-jets indicated that the unsteadiness intensity of the micro-jets and the shear stress in the cell is observed to be higher for 1-hole spacers than other perforated spacers, which explains the better flux and fouling reduction that 1-hole spacer provided. The same research group also evaluated the use the perforated spacers (with holes at filament intersections) in FO systems in another paper [117]. The perforated spacer was found to increase the permeate flux by 43% while the standard spacers showed 40% permeate flux increase when using water as feed and 0.6 M NaCl as draw solution. However, when using Shale Gas Produced Water (SGPW) as feed solution, the perforated spacers exhibited severe flux decline due to the presence of holes that aided the scaling coverage on the membrane area. The benefit of the holes on the perforated spacers lies in its capacity to minimize energy consumption, which was reflected by no pressure drop increase while incorporating the spacer. The presence of the holes on the spacer filament intersections also improved the cleaning efficiency since they provided a strong fluid shear force. Compared with the pressure driven process, the use of perforated spacers in FO showed less improvements on flux increase and fouling mitigation since these holes could generate stronger flow turbulence at higher pressure. The driving force of FO primarily came from concentration gradient, which is unable to promote the turbulence compared with higher external pressure.

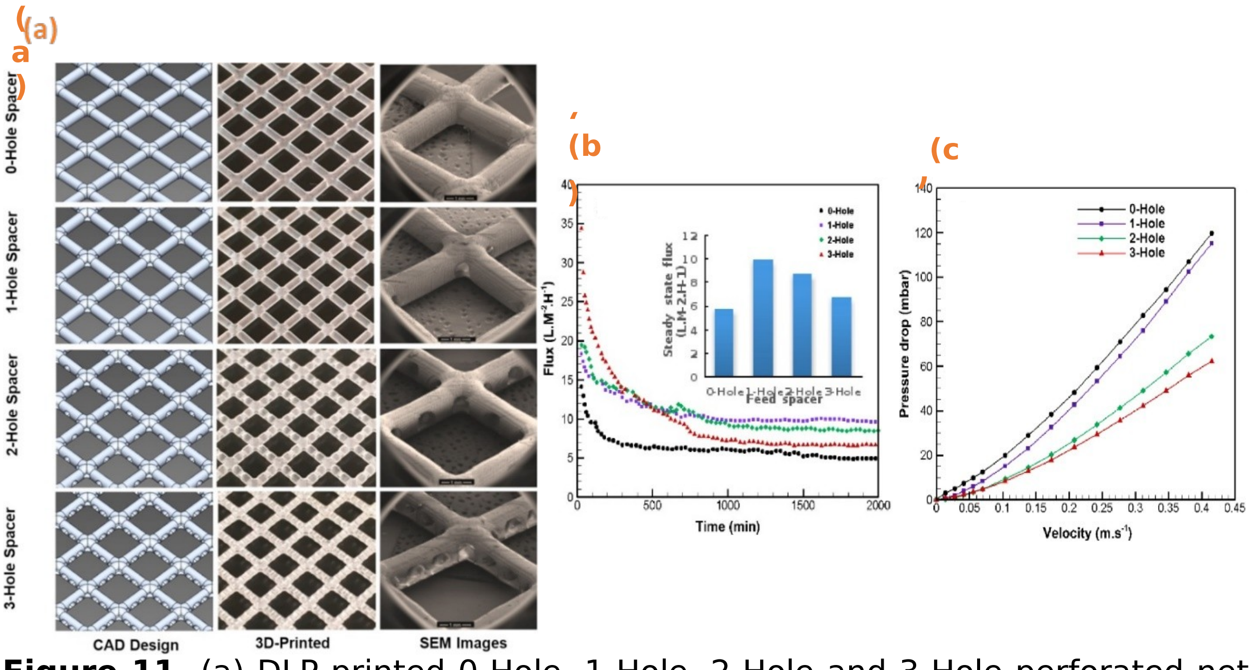

Figure 11. (a) DLP printed 0-Hole, 1-Hole, 2-Hole and 3-Hole perforated net spacers. (b) Long-term permeate flux in a UF crossflow cell with different spacers installed. Seawater was used as feed solution with constant initial pressure (60 kPa). (c) Feed channel pressure drop as a function of average crossflow velocity. Reproduced from [116]. This figure is best viewed in color.

Ali et al. [6] improved the spacer performance by reducing the thickness of spacer filament. With a thinner spacer filament that increased the clearance between the filament and membranes, the novel column spacers had the same structure and dimensions as the standard non-woven symmetric spacer, as shown in Figure 12(a). The column spacers were printed by DLP using acrylate monomer as printing material. The hydrodynamics in the flow channel was modeled by CFD and the spacer performance was tested in crossflow system on top of commercial UF membranes. Due to wider clearance zone, the flow velocity was significantly higher for the column spacer. This wider clearance zone also yielded to substantial reduction in pressure drop, shear stress and dead zone area. Based on the findings in Figure 12(b) and (c), the specific flux (flux produced per unit pressure drop) of the channel with column spacer was tested to be twice as high as the specific flux with the standard spacer at different crossflow velocity. Two-fold reduction in specific energy consumption (SEC, energy consumption to produce unit permeate flux) and three times lower pressure drop were observed for column spacer compared with standard spacer. Additionally, Optical Coherence Tomography (OCT) images demonstrated much less fouling layer accumulated on the membrane surface while incorporating the column spacer. This reduction in fouling agrees with the CFD results that stronger membrane washing was achieved by enlarging the clearance zone between membrane and filaments. In another work [118], the same research group printed novel hole-pillar spacer configuration with perforation on the spacer intersection by DLP. The spacer performance was analyzed in a UF crossflow setup at different operating pressures. Compared with the 3D printed net spacers, the hole-pillar spacers exhibited approximately 22% lower pressure drop than the net spacers. Additionally, the fluid velocity produced by the hole-pillar spacers is higher than that in the net spacers due to micro-jet formation by the perforation, which consequently eliminated the dead zone. This could also produce lower fouling for hole-pillar spacers. In terms of permeate flux in the UF test, hole-pillar spacers showed a 75% higher flux gain at 0.5 bar and 63% higher flux than net spacer at 1.0 bar. Ali et al. [119] demonstrated the use of DLP in printing turbospacers composed of a series of microturbines. Compared with conventional diamond spacers, the turbospacers showed approximately 15% lower flux decline, 2.5 times lower foulant resistance and 2 folds less pressure drop in the lab-scale FO experiment. The high performance of the turbospacers was due to the exploitation of the kinetic energy from the feed flow to rotate the turbines and create flow turbulence. Based on this advantage, the turbospacers were also used in low pressure UF process to reduce fouling formation [120]. Compared with standard symmetric non-woven spacers, the implementation of turbospacers lowered the average pressure drop by 4 times and increased the specific permeance flux by over 3 times in a 48-hr filtration test, which contributed to the 2.5 folds lower specific energy consumption for the turbospacers. The OCT images also demonstrated minimized accumulation of foulants by using turbospacers during the UF experiment.

Based on the above work, the DLP technique is able to print the spacers with a more complex configuration due to its higher resolution and precision. However, this method is limited to photopolymer resins. Currently, only acrylate monomers have been successfully printed into feed spacers via this technique.

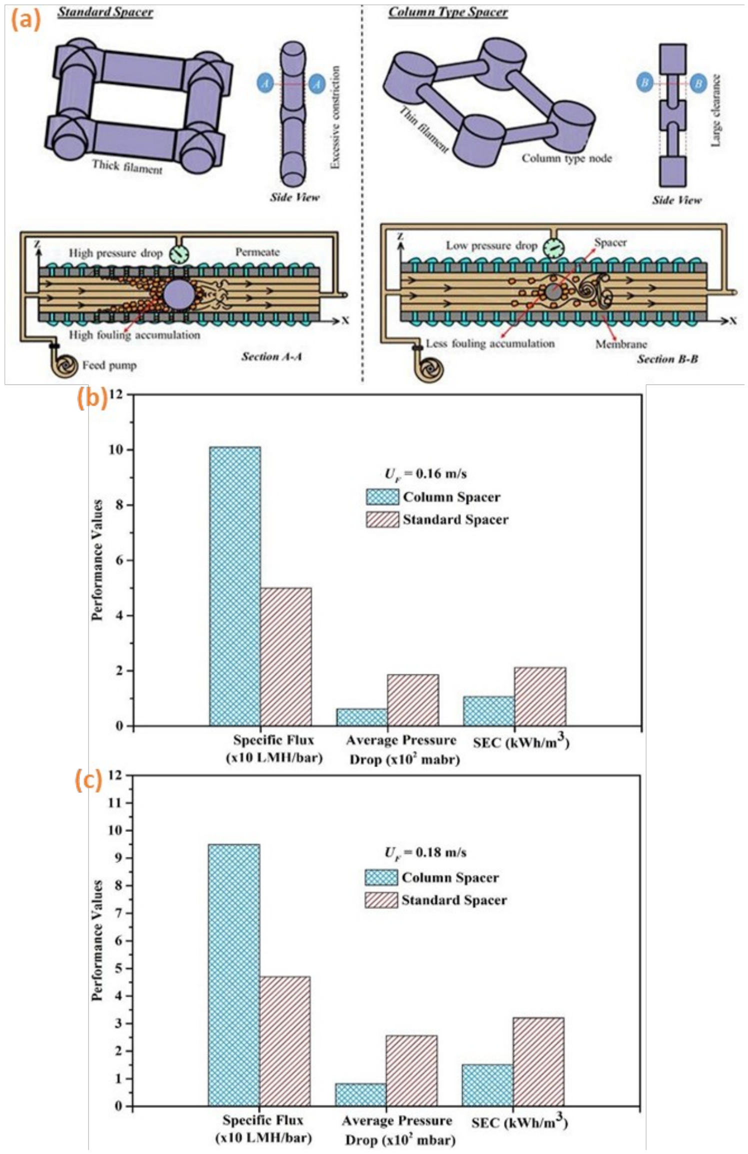

Figure 12. (a) DLP printed standard net-type spacers and column-type spacers and their corresponding fouling pattern in crossflow cell. Comparison on specific flux, average pressure drop and SEC for crossflow cells with column and standard spacers at 0.16 m/s (b) and 0.18m/s (c). (d). DLP printed turbospacer and its lower foulant resistance in FO. Reproduced from [6,119]. This figure is best viewed in color.

5. Discussion

Most of the efforts described here have focused on improving spacer design through the use of intricate structures that are non-manufacturable using conventional approaches. These designs are intended to yield specific performance benefits such as improved mixing (to lower CP and fouling) along with reduced pressure drop. Some of these structures (TPMS) were designed with mathematically proven minimal internal surface to reduce pressure drop and increase flow turbulence [46]. Others with novel shapes (helical [4], herringbone [108], perforated [116] etc.) could help shape the flow field, based on proper CFD simulation, thereby improving mixing, mass transfer and reduce fouling. All these novel structures benefited spacer performance due to their “flow friendly” configurations. Such spacers could have value in liquid filtration processes such as MF, UF, NF, FO, RO, and MD if they could be made in a scalable and inexpensive way.

Based on the review above, many printed spacers used in pressure-driven process are tested under low pressure condition such as UF. However, in reality spacers are commonly used in RO processes that requires higher pressure. 3D printed spacers are usually designed for specific purposes. For example, the TPMS structure demonstrated by Sreedhar et al. [46] designed for BWRO and UF to reduce pressure drop and biofilm development. The perforated spacers proposed by Kerdi et al. [116] and the turbospacers proposed by Ali et al. [120] are predominantly used for fouling mitigation of low pressure membrane filtration. It is recommended that 3D printed spacers could allow for a wider range of pressure tolerance in order to be used in higher pressure processes. This could impose higher level of requirements on the printed spacers to reduce pressure drop and fouling at a much higher operating pressure.

It is noticeable that most of the 3D printed spacers discussed above are made and tested at lab-scale, and scale-up challenges are generally observed in terms of spacer manufacturing and module performance. For example, the build–up volume of a typical DLP printer is 132 × 74 × 130 mm, with a printing speed at 80 mm/hr [121]. The largest SLA printer is capable of handling 2100 × 700 × 800 mm build volume [121]. However, most membrane modules require membrane area to be above 20 m^2, which exceeds the dimensions of most 3D printed spacers. On the other hand, many 3D printed spacers are only tested and modeled at lab scale. Scaling up in a real membrane module could indicate a completely different flow field, which leads to unpredicted mass transfer, pressure drop and fouling behavior.

We did notice a gap in one performance metric throughout these studies: spacer deformation. When designing spacer structures, most studies did not take into consideration issues such as the embossing of the membrane on the spacer (particularly for permeate spacers). Lee et al. [122] demonstrated that membranes could stretch for more open feed spacer constructions, but permeate spacer embossing is a problem for higher pressure membrane processes, particularly at higher pressures or with more open spacers [7]. Embossing can cause membrane stretching and can lead to defect formation and loss of selectivity. Much of this gap can be attributed to the general focus on feed spacers for new spacer designs rather than permeate spacers.

A research opportunity may be to develop spacers that can adapt to dynamic operation of modules. Compaction of the membrane in higher pressure environments may open up the feed channel and allow spacers to shift or vibrate. This movement may damage the membrane through abrasion, which in turn, causes a loss of selectivity. This issue highlights the need to address the surface finish of printed spacer technology, since rough spacer surfaces will be more prone to abrade the membrane surface. Largely absent from the papers we reviewed, improved surface finish is critically important since the spacer will contact the membrane during module assembly and operation.

Due to these issues, commercial viability of 3D printed spacers remains a question. The commercial risks for considering printed spacers go beyond just questions about deformation and surface finish, which have yet to be fully assessed by the research community. Cost remains a primary concern. Based on the study conducted by Tan et al. [76] and results in section 3, FDM is a likely candidate for making spacers with the advantages of additive manufacturing combined with commercial viability. However, we found that most of the studies reviewed here focused entirely on spacer performance with little discussion on commercial viability. It is evident that additive manufacturing is not an inexpensive method of making spacers for membrane processes that are used at large scales. Looking back a few decades, Da Costa et al. [13,14,37] did some cost analysis for conventional spacer designs, but these efforts have not translated to spacers manufactured through 3D printing. Liang et al. [123] used a techno-economic model to evaluate the total processing of multi-layer spacers in SWM module based on the mass transfer and pressure drop obtained from CFD model. The total SWM module processing cost derived from techno-economic model was composed of pretreatment cost, capital unit cost that included both membrane and spacer cost, energy cost which included both the energy used to generate inlet pressure and energy consumed by pressure loss. They demonstrated that the cost associated with pressure drop of multi-layered spacers in long channels was negligible. This study provided a convincing module processing cost, but did not address the manufacturing cost of spacers. In particular, the slow manufacturing speed of additive manufacturing leads to higher unit cost. In addition, most of these studies did not discuss other commercial viability metrics such as manufacturing size, TRL, and how much hazardous waste they produce. These drawbacks offset the value proposition of using exotic geometries that, while interesting, seem to be more of a scientific exploration rather than impactful technology development.

One 3D printed spacer technology has been commercialized. AquaMembranes has developed a process that enables the printing of spacers *directly onto an RO membrane* rather than as a standalone spacer [124,125]. These spacer-imprinted RO membranes have been assembled into spiral wound modules. The printed spacers enable the use of more densely packed membranes into spiral wound modules and have been shown to increase the membrane area of a typical 4040 or 8040 module by up to 40% over conventional with a commensurate increase in module permeate flow [126]. Additionally, the printed spacer pattern showed lower pressure drop that, they claim, could bring a potential annual global energy saving of $1.4 billion [127].

What is particularly interesting about this approach is that they, amongst many others cited in this review, are focusing on a high volume yet low value product of water. In the water space, the levelized cost of water is quite sensitive to the membrane module cost. This suggests that their process may not be too expensive as to drastically change the cost of the module overall. We will note that other membrane processes that involve the production of purification of higher value chemicals (e.g., industrial gases, organic liquids, foods and pharmaceuticals) may be less sensitive to the module price, and therefore, tolerate higher overall module costs when using exotic spacers. The benefits of these spacers may also be more prominent when using compressible fluids like gases or higher viscosity fluids.

6. Conclusions and Future Directions

This review summarizes a broad range of 3D printing techniques for spacers used in membrane processes for liquid separations. These studies have largely focused on increasing mixing and mass transfer while lowering pressure drop, CP and fouling propensity. These studies have achieved these goals through the use of exotic spacer geometries that cannot be manufactured using conventional manufacturing processes. While these efforts have produced interesting science and supported the development of computational tools for predicting mass transfer in membrane modules, much work is needed to bridge these studies to commercial products. It may be prudent to consider spacer options for higher value products or for cases where mass transfer limitations are limiting factors for module performance

Even with the critique above, there are opportunities for lab-scale research with spacers. Spacers offer a unique opportunity to access the interior of a membrane module with chemistry or other stimuli. There have already been uses of spacers to deliver anti-fouling chemistry to module feed channels. Other chemistries may likewise be deliverable to the feed channel through feed spacers. Proposing these types of approaches would need to demonstrate a clear value proposition to the separation application that they would be supporting and show a clear opportunity for manufacturability.

There are additional opportunities in stimuli-responsive materials that can adapt to variable conditions. The emergent field of 4D printed materials [128] offer unique opportunities for spacers to adapt to changing conditions within a membrane module. If we can create spacers that offer controllable pressure drop, mass transfer, and CP using responsive deformation, membrane modules may be adaptable to changing operating conditions. 4D printing combines 3D printing with smart materials to produce different devices, such as electro-responsive shape-changing sensors [129], thermal-responsive robotic actuators [130] and shape memory occlusion devices [131]. 4D printing has also been successful in forming light-responsive membranes, and it would be interesting to see if light or other stimuli could be incorporated into modules to change how membranes, or spacers, might behave in changing conditions. Other stimuli, such as electric or magnetic fields would be interesting to explore given the recent emergence of electromembrane processes [132–135]. There may be opportunities for spacers to play a role in these types of processes. Additive manufacturing may play a key role in developing these kinds of materials and structures.

With opportunities for new science around spacer design continuing to emerge, the field of spacer design is quite active in the research community. However, it is imperative that we identify high value opportunities for spacer design and utilization in membrane processes in order to overcome the inherent limitations of additive manufacturing. Innovations in additive manufacturing that drive down cost and increase speed may also enable broader use of 3D printed spacers. With such innovations, many of the concepts described here may begin to see commercial use over time leading to numerous and valuable benefits.

Authors Declaration

The authors declare this manuscript has been approved by all named authors. Every person contributing to this manuscript and satisfying the authorship has been listed. We also declare that we have followed the intellectual property regulations of our institutions and there are no impediments to publication in terms of intellectual property.

Conflict of Interest Statement

The authors declare that they have no known conflicts of interests or other relevant relationships that could impact the information in this paper.

Sources of Funding

Funding provided by the National Science Foundation (CMMI #2001544) and the National Alliance for Water Innovation (NAWI) funded by the U.S. Department of Energy, Office of Energy Efficiency and Renewable Energy (EERE), Advanced Manufacturing Office, under Funding Opportunity Announcement Number DE-FOA-0001905. Additional financial support for EMVH was provided by the UCLA Sustainable LA Grand Challenge.

Acknowledgements

We are grateful to Dr. Jinwen Wang at PolyCera Membranes for providing pricing ranges for commercial feed spacer materials.

References

[1] M. Mulder, Basic Principles of Membrane Technology, 1st ed., Springer Netherlands, 1991. https://doi.org/10.1007/978-94-017-0835-7.

[2] R.W. Baker, Membrane Technology and Applications, 3rd Edition, 3rd ed., John Wiley & Sons Ltd, Newark, California, USA, 2012.

[3] B. Gu, C.S. Adjiman, X.Y. Xu, The effect of feed spacer geometry on membrane performance and concentration polarisation based on 3D CFD simulations, J. Memb. Sci. 527 (2017) 78–91. https://doi.org/10.1016/j.memsci.2016.12.058.

[4] C. Fritzmann, M. Wiese, T. Melin, M. Wessling, Helically microstructured spacers improve mass transfer and fractionation selectivity in ultrafiltration, J. Memb. Sci. 463 (2014) 41–48. https://doi.org/10.1016/j.memsci.2014.03.059.

[5] N. Thomas, N. Sreedhar, O. Al-Ketan, R. Rowshan, R.K. Abu Al-Rub, H. Arafat, 3D printed spacers based on TPMS architectures for scaling control in membrane distillation, J. Memb. Sci. 581 (2019) 38–49. https://doi.org/10.1016/j.memsci.2019.03.039.

[6] S.M. Ali, A. Qamar, S. Kerdi, S. Phuntsho, J.S. Vrouwenvelder, N. Ghaffour, H.K. Shon, Energy efficient 3D printed column type feed spacer for membrane filtration, Water Res. 164 (2019). https://doi.org/10.1016/j.watres.2019.114961.

[7] C. Kleffner, G. Braun, S. Antonyuk, Influence of Membrane Intrusion on Permeate-Sided Pressure Drop During High-Pressure Reverse Osmosis,

Chemie-Ingenieur-Technik. 91 (2019) 443–454. https://doi.org/10.1002/cite.201800104.

[8] C.P. Koutsou, A.J. Karabelas, M. Kostoglou, Membrane desalination under constant water recovery - The effect of module design parameters on system performance, Sep. Purif. Technol. 147 (2015) 90–113. https://doi.org/10.1016/j.seppur.2015.04.012.

[9] C.P. Koutsou, A.J. Karabelas, T.B. Goudoulas, Characteristics of permeate-side spacers of spiral wound membrane modules, Desalination. 322 (2013) 131–136. https://doi.org/10.1016/j.desal.2013.05.015.

[10] A.H. Haidari, S.G.J. Heijman, W.G.J. van der Meer, Optimal design of spacers in reverse osmosis, Sep. Purif. Technol. 192 (2018) 441–456. https://doi.org/10.1016/j.seppur.2017.10.042.

[11] E.M.V. Hoek, J. Allred, T. Knoell, B.H. Jeong, Modeling the effects of fouling on full-scale reverse osmosis processes, J. Memb. Sci. 314 (2008) 33–49. https://doi.org/10.1016/j.memsci.2008.01.025.

[12] Z. Cao, D.E. Wiley, A.G. Fane, CFD simulations of net-type turbulence promoters in a narrow channel, J. Memb. Sci. 185 (2001) 157–176. https://doi.org/10.1016/S0376-7388(00)00643-8.

[13] A.R. Da Costa, A.G. Fane, C.J.D. Fell, A.C.M. Franken, Optimal channel spacer design for ultrafiltration, J. Memb. Sci. 62 (1991) 275–291. https://doi.org/10.1016/0376-7388(91)80043-6.

[14] A.R. Da Costa, A.G. Fane, D.E. Wiley, Spacer characterization and

pressure drop modeling in spacer-filled channels.pdf, J. Memb. Sci. 87 (1994) 79–98.

[15] H.S. Abid, D.J. Johnson, R. Hashaikeh, N. Hilal, A review of efforts to reduce membrane fouling by control of feed spacer characteristics, Desalination. 420 (2017) 384–402. https://doi.org/10.1016/j.desal.2017.07.019.

[16] P.A. Araújo, J.C. Kruithof, M.C.M. Van Loosdrecht, J.S. Vrouwenvelder, The potential of standard and modified feed spacers for biofouling control, J. Memb. Sci. 403–404 (2012) 58–70. https://doi.org/10.1016/j.memsci.2012.02.015.

[17] A.J. Karabelas, C.P. Koutsou, D.C. Sioutopoulos, Comprehensive performance assessment of spacers in spiral-wound membrane modules accounting for compressibility effects, J. Memb. Sci. 549 (2018) 602–615. https://doi.org/10.1016/j.memsci.2017.12.037.

[18] O. Kavianipour, G.D. Ingram, H.B. Vuthaluru, Investigation into the effectiveness of feed spacer configurations for reverse osmosis membrane modules using Computational Fluid Dynamics, J. Memb. Sci. 526 (2017) 156–171. https://doi.org/10.1016/j.memsci.2016.12.034.

[19] A.L. Ahmad, K.K. Lau, M.Z. Abu Bakar, Impact of different spacer filament geometries on concentration polarization control in narrow membrane channel, J. Memb. Sci. 262 (2005) 138–152. https://doi.org/10.1016/j.memsci.2005.06.056.

[20] V. V. Ranade, A. Kumar, Fluid dynamics of spacer filled rectangular and

curvilinear channels, J. Memb. Sci. 271 (2006) 1–15. https://doi.org/10.1016/j.memsci.2005.07.013.

[21] Z.X. Low, Y.T. Chua, B.M. Ray, D. Mattia, I.S. Metcalfe, D.A. Patterson, Perspective on 3D printing of separation membranes and comparison to related unconventional fabrication techniques, J. Memb. Sci. 523 (2017) 596–613. https://doi.org/10.1016/j.memsci.2016.10.006.

[22] L.D. Tijing, J.R.C. Dizon, I. Ibrahim, A.R.N. Nisay, H.K. Shon, R.C. Advincula, 3D printing for membrane separation, desalination and water treatment, Appl. Mater. Today. 18 (2020) 100486. https://doi.org/10.1016/j.apmt.2019.100486.

[23] J.Y. Lee, W.S. Tan, J. An, C.K. Chua, C.Y. Tang, A.G. Fane, T.H. Chong, The potential to enhance membrane module design with 3D printing technology, J. Memb. Sci. 499 (2016) 480–490. https://doi.org/10.1016/j.memsci.2015.11.008.

[24] J.W. Koo, J.S. Ho, J. An, Y. Zhang, C.K. Chua, T.H. Chong, A review on spacers and membranes: Conventional or hybrid additive manufacturing?, Water Res. 188 (2021) 116497. https://doi.org/10.1016/j.watres.2020.116497.

[25] J. Baker, T. Stephenson, S. Dard, P. Côté, Characterisation of fouling of nanofiltration membranes used to treatsurface waters, Environ. Technol. (United Kingdom). 16 (1995) 977–985. https://doi.org/10.1080/09593331608616335.

[26] H.L. Yang, J.C. Te Lin, C. Huang, Application of nanosilver surface

modification to RO membrane and spacer for mitigating biofouling in seawater desalination, Water Res. 43 (2009) 3777–3786. https://doi.org/10.1016/j.watres.2009.06.002.

[27] A. Ronen, S. Lerman, G.Z. Ramon, C.G. Dosoretz, Experimental characterization and numerical simulation of the anti-biofuling activity of nanosilver-modified feed spacers in membrane filtration, J. Memb. Sci. 475 (2015) 320–329. https://doi.org/10.1016/j.memsci.2014.10.042.

[28] A. Ronen, R. Semiat, C.G. Dosoretz, Impact of ZnO embedded feed spacer on biofilm development in membrane systems, Water Res. 47 (2013) 6628–6638. https://doi.org/10.1016/j.watres.2013.08.036.

[29] C. Thamaraiselvan, Y. Carmiel, G. Eliad, C.N. Sukenik, R. Semiat, C.G. Dosoretz, Modification of a polypropylene feed spacer with metal oxide-thin film by chemical bath deposition for biofouling control in membrane filtration, J. Memb. Sci. 573 (2019) 511–519. https://doi.org/10.1016/j.memsci.2018.12.033.

[30] R. Hausman, T. Gullinkala, I.C. Escobar, Development of Low-Biofouling Polypropylene Feedspacers for Reverse Osmosis, J. OfAppliedPolymer Sci. 114 (2009) 3068–3073.

[31] R. Hausman, I.C. Escobar, A comparison of silver- and copper-charged polypropylene feed spacers for biofouling control, J. Appl. Polym. Sci. 128 (2013) 1706–1714. https://doi.org/10.1002/app.38164.

[32] A. Ronen, A. Resnick, S. Lerman, M.S. Eisen, C.G. Dosoretz, Biofouling suppression of modified feed spacers: Localized and long-distance

antibacterial activity, Desalination. 393 (2016) 159–165. https://doi.org/10.1016/j.desal.2015.07.004.

[33] M. Jabłońska, M. Menzel, U. Hirsch, A. Heilmann, Assessment of anti-bacterial adhesion and anti-biofouling potential of plasma-mediated poly(sulfobetaine methacrylate) coatings of feed spacer, Desalination. 493 (2020).

[34] M. Elimelech, W.A. Phillip, The future of seawater desalination: Energy, technology, and the environment, Science (80-.). 333 (2011) 712–717. https://doi.org/10.1126/science.1200488.

[35] H. Kitano, K. Takeuchi, J. Ortiz-Medina, R. Cruz-Silva, A. Morelos-Gomez, M. Fujii, M. Obata, A. Yamanaka, S. Tejima, M. Fujishige, N. Akuzawa, A. Yamaguchi, M. Endo, Enhanced Antifouling Feed Spacer Made from a Carbon Nanotube-Polypropylene Nanocomposite, ACS Omega. 4 (2019) 15496–15503. https://doi.org/10.1021/acsomega.9b01757.

[36] V. Geraldes, V. Semião, M.N. De Pinho, Flow management in nanofiltration spiral wound modules with ladder-type spacers, J. Memb. Sci. 203 (2002) 87–102. https://doi.org/10.1016/S0376-7388(01)00753-0.

[37] A.R. Da Costa, A.G. Fane, Net-Type Spacers: Effect of Configuration on Fluid Flow Path and Ultrafiltration Flux, Ind. Eng. Chem. Res. 33 (1994) 1845–1851. https://doi.org/10.1021/ie00031a026.

[38] H.G. Park, S.G. Cho, K.J. Kim, Y.N. Kwon, Effect of feed spacer thickness on the fouling behavior in reverse osmosis process - A pilot scale study,

Desalination. 379 (2016) 155–163. https://doi.org/10.1016/j.desal.2015.11.011.

[39] F. Li, W. Meindersma, A.B. De Haan, T. Reith, Experimental validation of CFD mass transfer simulations in flat channels with non-woven net spacers, J. Memb. Sci. 232 (2004) 19–30. https://doi.org/10.1016/j.memsci.2003.11.015.

[40] F. Li, W. Meindersma, A.B. De Haan, T. Reith, Optimization of commercial net spacers in spiral wound membrane modules, J. Memb. Sci. 208 (2002) 289–302. https://doi.org/10.1016/S0376-7388(02)00307-1.

[41] C.P. Koutsou, S.G. Yiantsios, A.J. Karabelas, Direct numerical simulation of flow in spacer-filled channels: Effect of spacer geometrical characteristics, J. Memb. Sci. 291 (2007) 53–69. https://doi.org/10.1016/j.memsci.2006.12.032.

[42] M. Amokrane, D. Sadaoui, M. Dudeck, C.P. Koutsou, New spacer designs for the performance improvement of the zigzag spacer configuration in spiral-wound membrane modules, Desalin. Water Treat. 57 (2016) 5266–5274. https://doi.org/10.1080/19443994.2015.1022003.

[43] A.I. Radu, J.S. Vrouwenvelder, M.C.M. van Loosdrecht, C. Picioreanu, Modeling the effect of biofilm formation on reverse osmosis performance: Flux, feed channel pressure drop and solute passage, J. Memb. Sci. 365 (2010) 1–15. https://doi.org/10.1016/j.memsci.2010.07.036.

[44] F. Li, W. Meindersma, A.B. De Haan, T. Reith, Novel spacers for mass transfer enhancement in membrane separations, J. Memb. Sci. 253 (2005) 1–12. https://doi.org/10.1016/j.memsci.2004.12.019.

[45] N. Thomas, N. Sreedhar, O. Al-Ketan, R. Rowshan, R.K. Abu Al-Rub, H. Arafat, 3D printed triply periodic minimal surfaces as spacers for enhanced heat and mass transfer in membrane distillation, Desalination. 443 (2018) 256–271. https://doi.org/10.1016/j.desal.2018.06.009.

[46] N. Sreedhar, N. Thomas, O. Al-Ketan, R. Rowshan, H. Hernandez, R.K. Abu Al-Rub, H.A. Arafat, 3D printed feed spacers based on triply periodic minimal surfaces for flux enhancement and biofouling mitigation in RO and UF, Desalination. 425 (2018) 12–21. https://doi.org/10.1016/j.desal.2017.10.010.

[47] N. Thomas, J. Swaminathan, G. Zaragoza, R.K. Abu Al-Rub, J.H. Lienhard V, H.A. Arafat, Comparative assessment of the effects of 3D printed feed spacers on process performance in MD systems, Desalination. 503 (2021) 114940. https://doi.org/10.1016/j.desal.2021.114940.

[48] N. Sreedhar, N. Thomas, O. Al-Ketan, R. Rowshan, R.K. Abu Al-Rub, S. Hong, H.A. Arafat, Impacts of feed spacer design on UF membrane cleaning efficiency, J. Memb. Sci. 616 (2020) 118571. https://doi.org/10.1016/j.memsci.2020.118571.

[49] Y. Chen, H. Bin Zhang, M. Wang, X. Qian, A. Dasari, Z.Z. Yu, Phenolic resin-enhanced three-dimensional graphene aerogels and their epoxy

nanocomposites with high mechanical and electromagnetic interference shielding performances, Compos. Sci. Technol. 152 (2017) 254–262. https://doi.org/10.1016/j.compscitech.2017.09.022.

[50] O.G. Kravchenko, D. Pedrazzoli, D. Kovtun, X. Qian, I. Manas-Zloczower, Incorporation of plasma-functionalized carbon nanostructures in composite laminates for interlaminar reinforcement and delamination crack monitoring, J. Phys. Chem. Solids. 112 (2018) 163–170. https://doi.org/10.1016/j.jpcs.2017.09.018.

[51] X. Qian, O.G. Kravchenko, D. Pedrazzoli, I. Manas-Zloczower, Effect of polycarbonate film surface morphology and oxygen plasma treatment on mode I and II fracture toughness of interleaved composite laminates, Compos. Part A Appl. Sci. Manuf. 105 (2018) 138–149. https://doi.org/10.1016/j.compositesa.2017.11.016.

[52] O.G. Kravchenko, X. Qian, S.G. Kravchenko, R. Misiego, R.B. Pipes, I. Manas-Zloczower, Role of hierarchical morphology of helical carbon nanotube bundles on thermal expansion of polymer nanocomposites, J. Mater. Res. 32 (2017) 2738–2746. https://doi.org/10.1557/jmr.2017.214.

[53] W. See, 3D Printing of Feed Channel Spacers for Spiral Wound Membrane Modules 3D Printing of Feed Channel Spacers for Spiral Wound Membrane Modules, 2018. https://doi.org/doi.org/10.32657/10356/75017.

[54] J. Schwinge, D.E. Wiley, A.G. Fane, Novel spacer design improves

observed flux, J. Memb. Sci. 229 (2004) 53–61. https://doi.org/10.1016/j.memsci.2003.09.015.

[55] A. Lee, D.H. Kim, B. Kim, C.K. Shin, P. Lee, K. Min, Feed spacer having three-layered structure, and reverse osmosis membrane filter module including same, US 2020/0086276 A1, 2020.

[56] D.F.Heaney, Qualification of metal injection molding (MIM), in: Handb. Met. Inject. Molding, 2012: pp. 254–264.

[57] D.F. Heaney, Handbook of Metal Injection Molding, 2012.

[58] B.C. Mutsuddy, R.G. Ford, Ceramic injection molding, Chapman / Hall, 1994.

[59] A.C. Karmaker, J.A. Youngquist, Injection molding of polypropylene reinforced with short jute fibers, J. Appl. Polym. Sci. 62 (1996) 1147–1151.

[60] R.M. German, Powder injection molding, in: Rensselaer Polytech. Institute, Troy, New York, 1990. https://doi.org/10.1557/s0883769400059741.

[61] X. Qian, T. Ravindran, S.J. Lounder, A. Asatekin, J.R. McCutcheon, Printing zwitterionic self-assembled thin film composite membranes: Tuning thickness leads to remarkable permeability for nanofiltration, J. Memb. Sci. 635 (2021) 119428. https://doi.org/10.1016/j.memsci.2021.119428.

[62] Y. Fan, X. Wang, X. Qian, A. Dixit, B. Herman, Y. Lei, J. McCutcheon, B. Li, Enhancing the Understanding of Soil Nitrogen Fate Using a 3D-

Electrospray Sensor Roll Casted with a Thin-Layer Hydrogel, Environ. Sci. Technol. (2022). https://doi.org/10.1021/acs.est.1c05661.

[63] Y. Fan, X. Qian, X. Wang, T. Funk, B. Herman, J.R. McCutcheon, B. Li, Enhancing long-term accuracy and durability of wastewater monitoring using electrosprayed ultra-thin solid-state ion selective membrane sensors, J. Memb. Sci. 643 (2022) 119997. https://doi.org/10.1016/j.memsci.2021.119997.

[64] M.R. Chowdhury, J. Steffes, B.D. Huey, J.R. Mccutcheon, 3D printed polyamide membranes for desalination, Science (80-.). 361 (2018) 682–686.

[65] X. Qian, M. Ostwal, A. Asatekin, G.M. Geise, Z.P. Smith, W.A. Phillip, R.P. Lively, J.R. McCutcheon, A critical review and commentary on recent progress of additive manufacturing and its impact on membrane technology, J. Memb. Sci. 645 (2022) 120041. https://doi.org/10.1016/j.memsci.2021.120041.

[66] H. Dommati, S.S. Ray, J.C. Wang, S.S. Chen, A comprehensive review of recent developments in 3D printing technique for ceramic membrane fabrication for water purification, RSC Adv. 9 (2019) 16869–16883. https://doi.org/10.1039/c9ra00872a.

[67] M. Shakaib, S.M.F. Hasani, M. Mahmood, Study on the effects of spacer geometry in membrane feed channels using three-dimensional computational flow modeling, J. Memb. Sci. 297 (2007) 74–89. https://doi.org/10.1016/j.memsci.2007.03.010.

[68] R. Valladares Linares, S.S. Bucs, Z. Li, M. AbuGhdeeb, G. Amy, J.S. Vrouwenvelder, Impact of spacer thickness on biofouling in forward osmosis, Water Res. 57 (2014) 223–233. https://doi.org/10.1016/j.watres.2014.03.046.

[69] I. Grida, J.R.G. Evans, Extrusion freeforming of ceramics through fine nozzles, J. Eur. Ceram. Soc. 23 (2003) 629–635. https://doi.org/10.1016/S0955-2219(02)00163-2.

[70] T. Isobe, T. Tomita, Y. Kameshima, A. Nakajima, K. Okada, Preparation and properties of porous alumina ceramics with oriented cylindrical pores produced by an extrusion method, J. Eur. Ceram. Soc. 26 (2006) 957–960. https://doi.org/10.1016/j.jeurceramsoc.2004.11.015.

[71] W. Graessi, D. Gi, Die Swell in Molten Polymers, 544 (1970). https://doi.org/10.1122/1.549177.

[72] R. Ahmed, R.F. Liang, M.R. Mackley, The experimental observation and numerical prediction of planar entry flow and die swell for molten polyethylenes, J. Nonnewton. Fluid Mech. 59 (1995) 129–153. https://doi.org/10.1016/0377-0257(95)01358-3.

[73] J.Z. Liang, Effects of extrusion conditions on die-swell behavior of polypropylene/diatomite composite melts, Polym. Test. 27 (2008) 936–940. https://doi.org/10.1016/j.polymertesting.2008.08.001.

[74] J.S. Anand, I.S. Bhardwaj, Die swell behaviour of polypropylene - An experimental investigation, Rheol. Acta. 19 (1980) 614–622. https://doi.org/10.1007/BF01517515.

[75] D. Tang, F.H. Marchesini, L. Cardon, D.R. D’hooge, State of the-Art for Extrudate Swell of Molten Polymers: From Fundamental Understanding at Molecular Scale toward Optimal Die Design at Final Product Scale, Macromol. Mater. Eng. 305 (2020) 1–24. https://doi.org/10.1002/mame.202000340.

[76] W.S. Tan, S.R. Suwarno, J. An, C.K. Chua, A.G. Fane, T.H. Chong, Comparison of solid, liquid and powder forms of 3D printing techniques in membrane spacer fabrication, J. Memb. Sci. 537 (2017) 283–296. https://doi.org/10.1016/j.memsci.2017.05.037.

[77] J. O’Connell, Fast 3D Prints: How to Increase Your 3D Printing Speed, (2021).

[78] Membrane shapes and modules, (n.d.). http://www.separationprocesses.com/Membrane/MT_Chp04a.htm.

[79] PVDF membrane filter roll stock, TISCH Sci. (n.d.). https://scientificfilters.com/roll-stock-membranes/pvdf.

[80] Reverse Osmosis (RO) Membranes, Sterlitech Corp. (n.d.). https://www.sterlitech.com/reverse-osmosis-ro-membrane.html.

[81] HJC raw materials polyamide membrane 100gpd for ro membrane reverse osmosis flat sheet, (n.d.). https://www.alibaba.com/product-detail/Membrane-Ro-Flat-Sheet-Membrane-For_1600281871256.html?spm=a2700.7724857.normal_offer.d_title.73f9313173zOuQ&s=p.

[82] Typical Flexural Strength and Flexural Modulus of Polymers, (n.d.). http://www.matweb.com/reference/flexuralstrength.aspx.

[83] Stratasys Systems, Digital ABS Plus, 2018.

[84] EOS GmbH - Electro Optical Systems Product, PA 2200 Performance 1.0, 2010.

[85] Stratasys, Vero Clear: Rigid Transparent 3D Printing Material, 2020. https://www.stratasys.com/materials/search/veroclear.

[86] J.H. Schut, High-Speed Extrusion: Are You Ready for the Fast Lane?, 2008. https://www.ptonline.com/articles/high-speed-extrusion-are-you-ready-for-the-fast-lane.

[87] J. Molenaar, R.J. Koopmans, C.F.J. den Doelder, Onset of the sharkskin phenomenon in polymer extrusion, Phys. Rev. E. 58 (1998) 4683–4691.

[88] J.M. Piau, N. El Kissi, B. Tremblay, Influence of upstream instabilities and wall slip on melt fracture and sharkskin phenomena during silicones extrusion through orifice dies, J. Nonnewton. Fluid Mech. 34 (1990) 145–180. https://doi.org/10.1016/0377-0257(90)80016-S.

[89] N. El Kissi, J.M. Piau, F. Toussaint, Sharkskin and cracking of polymer melt extrudates, J. Nonnewton. Fluid Mech. 68 (1997) 271–290. https://doi.org/10.1016/s0377-0257(96)01507-8.

[90] J. Unwin, M.R. Coldwell, C. Keen, J.J. McAlinden, Airborne emissions of carcinogens and respiratory sensitizers during thermal processing of plastics, Ann. Occup. Hyg. 57 (2013) 399–406. https://doi.org/10.1093/annhyg/mes078.

[91] J. Sims, P.A. Ellwood, H.J. Taylor, Pollutants from laser cutting and hot gas welding of polymer based materials, Annu. Tech. Conf. - ANTEC,

Conf. Proc. (1994) 1269–1273.

[92] P. Steinle, Characterization of emissions from a desktop 3D printer and indoor air measurements in office settings, J. Occup. Environ. Hyg. 13 (2016) 121–132. https://doi.org/10.1080/15459624.2015.1091957.

[93] P. Azimi, D. Zhao, C. Pouzet, N.E. Crain, B. Stephens, Emissions of Ultrafine Particles and Volatile Organic Compounds from Commercially Available Desktop Three-Dimensional Printers with Multiple Filaments, Environ. Sci. Technol. 50 (2016) 1260–1268. https://doi.org/10.1021/acs.est.5b04983.

[94] NASA, Technology Readiness Level Definitions, (1989) 1. https://www.nasa.gov/pdf/458490main_TRL_Definitions.pdf.

[95] R. Lezama-Nicolás, M. Rodríguez-Salvador, R. Río-Belver, I. Bildosola, A bibliometric method for assessing technological maturity: the case of additive manufacturing, Scientometrics. 117 (2018) 1425–1452. https://doi.org/10.1007/s11192-018-2941-1.

[96] G. Pratofiorito, H. Horn, F. Saravia, Differentiating fouling on the membrane and on the spacer in low-pressure reverse-osmosis under high organic load using optical coherence tomography, Sep. Purif. Technol. 291 (2022) 120885. https://doi.org/10.1016/j.seppur.2022.120885.

[97] O. Jung, F. Saravia, M. Wagner, S. Heißler, H. Horn, Quantifying Concentration Polarization – Raman Microspectroscopy for In-Situ Measurement in a Flat Sheet Cross-flow Nanofiltration Membrane Unit,

Sci. Rep. 9 (2019) 1–11. https://doi.org/10.1038/s41598-019-52369-1.

[98] B. Gu, C.S. Adjiman, X.Y. Xu, Correlations for concentration polarization and pressure drop in spacer-filled RO membrane modules based on CFD simulations, Membranes (Basel). 11 (2021). https://doi.org/10.3390/membranes11050338.

[99] J. Balster, I. Pünt, D.F. Stamatialis, M. Wessling, Multi-layer spacer geometries with improved mass transport, J. Memb. Sci. 282 (2006) 351–361. https://doi.org/10.1016/j.memsci.2006.05.039.

[100] F. Li, A. Haan, G. Meindersma, T. Reith, Spacer for use in a membrane separation device and a membrane separation device comprising such a spacer, 2004.

[101] H. Schwarz, Gesammelte Mathematische Abhandlungen, Springer, Berlin, 1933.

[102] A.H. Schoen, Infinite periodic minimal surfaces without self-intersections, Nasa Tech. Note D-5541. (1970) 92. http://ntrs.nasa.gov/search.jsp?R=19700020472.

[103] N. Thomas, M. Kumar, G. Palmisano, R.K.A. Al-Rub, R.Y. Alnuaimi, E. Alhseinat, R. Rowshan, H.A. Arafat, Antiscaling 3D printed feed spacers via facile nanoparticle coating for membrane distillation, Water Res. 189 (2021) 116649. https://doi.org/10.1016/j.watres.2020.116649.

[104] E.H.C. Castillo, N. Thomas, O. Al-Ketan, R. Rowshan, R.K. Abu Al-Rub, L.D. Nghiem, S. Vigneswaran, H.A. Arafat, G. Naidu, 3D printed spacers for organic fouling mitigation in membrane distillation, J. Memb. Sci.

581 (2019) 331–343. https://doi.org/10.1016/j.memsci.2019.03.040.
[105] W.S. Tan, C.K. Chua, T.H. Chong, A.G. Fane, A. Jia, 3D printing by selective laser sintering of polypropylene feed channel spacers for spiral wound membrane modules for the water industry, Virtual Phys. Prototyp. 11 (2016) 151–158. https://doi.org/10.1080/17452759.2016.1211925.
[106] S. Park, Y.D. Jeong, J.H. Lee, J. Kim, K. Jeong, K.H. Cho, 3D printed honeycomb-shaped feed channel spacer for membrane fouling mitigation in nanofiltration, J. Memb. Sci. 620 (2021) 118665. https://doi.org/10.1016/j.memsci.2020.118665.
[107] Y.Z. Tan, Z. Mao, Y. Zhang, W.S. Tan, T.H. Chong, B. Wu, J.W. Chew, Enhancing fouling mitigation of submerged flat-sheet membranes by vibrating 3D-spacers, Sep. Purif. Technol. 215 (2019) 70–80. https://doi.org/10.1016/j.seppur.2018.12.085.
[108] A. Shrivastava, S. Kumar, E.L. Cussler, Predicting the effect of membrane spacers on mass transfer, J. Memb. Sci. 323 (2008) 247–256. https://doi.org/10.1016/j.memsci.2008.05.060.
[109] N. Yanar, M. Son, E. Yang, Y. Kim, H. Park, S.E. Nam, H. Choi, Investigation of the performance behavior of a forward osmosis membrane system using various feed spacer materials fabricated by 3D printing technique, Chemosphere. 202 (2018) 708–715. https://doi.org/10.1016/j.chemosphere.2018.03.147.
[110] N. Yanar, M. Son, H. Park, H. Choi, Bio-mimetically inspired 3D-printed

honeycombed support (spacer) for the reduction of reverse solute flux and fouling of osmotic energy driven membranes, J. Ind. Eng. Chem. 83 (2020) 343–350. https://doi.org/10.1016/j.jiec.2019.12.007.

[111] A. Siddiqui, N. Farhat, S.S. Bucs, R.V. Linares, C. Picioreanu, J.C. Kruithof, M.C.M. Van Loosdrecht, J. Kidwell, J.S. Vrouwenvelder, Development and characterization of 3D-printed feed spacers for spiral wound membrane systems, Water Res. 91 (2016) 55–67. https://doi.org/10.1016/j.watres.2015.12.052.

[112] S. Kerdi, A. Qamar, A. Alpatova, J.S. Vrouwenvelder, N. Ghaffour, Membrane filtration performance enhancement and biofouling mitigation using symmetric spacers with helical filaments, Desalination. 484 (2020) 114454. https://doi.org/10.1016/j.desal.2020.114454.

[113] C. Fritzmann, M. Hausmann, M. Wiese, M. Wessling, T. Melin, Microstructured spacers for submerged membrane filtration systems, J. Memb. Sci. 446 (2013) 189–200. https://doi.org/10.1016/j.memsci.2013.06.033.

[114] B. Van Dang, A.J. Charlton, Q. Li, Y.C. Kim, R.A. Taylor, P. Le-Clech, T. Barber, Can 3D-printed spacers improve filtration at the microscale?, Sep. Purif. Technol. 256 (2021) 117776. https://doi.org/10.1016/j.seppur.2020.117776.

[115] J. Liu, A. Iranshahi, Y. Lou, G. Lipscomb, Static mixing spacers for spiral wound modules, J. Memb. Sci. 442 (2013) 140–148. https://doi.org/10.1016/j.memsci.2013.03.063.

[116] S. Kerdi, A. Qamar, J.S. Vrouwenvelder, N. Ghaffour, Fouling resilient perforated feed spacers for membrane filtration, Water Res. 140 (2018) 211–219. https://doi.org/10.1016/j.watres.2018.04.049.

[117] J. AlQattan, Y. Kim, S. Kerdi, A. Qamar, N. Ghaffour, Hole-type spacers for more stable shale gas-producedwater treatment by forward osmosis, Membranes (Basel). 11 (2021) 1–16. https://doi.org/10.3390/membranes11010034.

[118] A. Qamar, S. Kerdi, S.M. Ali, H.K. Shon, J.S. Vrouwenvelder, N. Ghaffour, Novel hole-pillar spacer design for improved hydrodynamics and biofouling mitigation in membrane filtration, Sci. Rep. 11 (2021) 1–13. https://doi.org/10.1038/s41598-021-86459-w.

[119] S.M. Ali, Y. Kim, A. Qamar, G. Naidu, S. Phuntsho, N. Ghaffour, J.S. Vrouwenvelder, H.K. Shon, Dynamic feed spacer for fouling minimization in forward osmosis process, Desalination. 515 (2021) 115198. https://doi.org/10.1016/j.desal.2021.115198.

[120] S.M. Ali, A. Qamar, S. Phuntsho, N. Ghaffour, J.S. Vrouwenvelder, H.K. Shon, Conceptual design of a dynamic turbospacer for efficient low pressure membrane filtration, Desalination. 496 (2020) 114712. https://doi.org/10.1016/j.desal.2020.114712.

[121] A. Soo, S.M. Ali, H.K. Shon, 3D printing for membrane desalination: Challenges and future prospects, Desalination. 520 (2021) 115366. https://doi.org/10.1016/j.desal.2021.115366.

[122] C. Lee, J. Jang, N.T. Tin, S. Kim, C.Y. Tang, I.S. Kim, Effect of Spacer

Configuration on the Characteristics of FO Membranes: Alteration of Permeation Characteristics by Membrane Deformation and Concentration Polarization, Environ. Sci. Technol. 54 (2020) 6385–6395. https://doi.org/10.1021/acs.est.9b06921.

[123] Y.Y. Liang, K.Y. Toh, G.A. Fimbres Weihs, 3D CFD study of the effect of multi-layer spacers on membrane performance under steady flow, J. Memb. Sci. 580 (2019) 256–267. https://doi.org/10.1016/j.memsci.2019.02.015.

[124] R. Kevin, H. Rodney, Graded Spacers for filtration wound elements, 2018.

[125] K. Roderick, R. Herrington, Improved Spiral Wound Element Construction, 2014.

[126] R.E. Herrington, Performance of super enhanced permeate flow RO elements with 3D spacers printed directly on the membrane surface, Proc. Membr. Technol. Conf. Expo. (2018) 1–22.

[127] A. Membranes, Aqua Membranes Printed Spacer Technology Patented Game Changing Innovation in Reverse Osmosis Technology, n.d.

[128] P. Fu, H. Li, J. Gong, Z. Fan, A.T. Smith, K. Shen, T.O. Khalfalla, H. Huang, X. Qian, J.R. McCutcheon, L. Sun, 4D printing of polymers: Techniques, materials, and prospects, Prog. Polym. Sci. 126 (2022) 101506. https://doi.org/10.1016/j.progpolymsci.2022.101506.

[129] X. Wan, F. Zhang, Y. Liu, J. Leng, CNT-based electro-responsive shape memory functionalized 3D printed nanocomposites for liquid sensors,

Carbon N. Y. 155 (2019) 77–87. https://doi.org/10.1016/j.carbon.2019.08.047.

[130] A.K. Mishra, T.J. Wallin, W. Pan, P. Xu, K. Wang, E.P. Giannelis, B. Mazzolai, R.F. Shepherd, Autonomic perspiration in 3D-printed hydrogel actuators, Sci. Robot. 5 (2020) 1–10. https://doi.org/10.1126/scirobotics.aaz3918.

[131] C. Lin, J. Lv, Y. Li, F. Zhang, J. Li, Y. Liu, L. Liu, J. Leng, 4D-Printed Biodegradable and Remotely Controllable Shape Memory Occlusion Devices, Adv. Funct. Mater. 29 (2019) 1–10. https://doi.org/10.1002/adfm.201906569.

[132] N. Drouin, P. Kubáň, S. Rudaz, S. Pedersen-Bjergaard, J. Schappler, Electromembrane extraction: Overview of the last decade, TrAC - Trends Anal. Chem. 113 (2019) 357–363. https://doi.org/10.1016/j.trac.2018.10.024.

[133] R.K. Nagarale, G.S. Gohil, V.K. Shahi, Recent developments on ion-exchange membranes and electro-membrane processes, Adv. Colloid Interface Sci. 119 (2006) 97–130. https://doi.org/10.1016/j.cis.2005.09.005.

[134] N. Kabay, O. Arar, S. Bunani, Water Treatment by Electromembrane Processes, in: Emerg. Membr. Technol. Sustain. Water Treat., Elsevier B.V., 2016: pp. 181–214.

[135] L. Handojo, A.K. Wardani, D. Regina, C. Bella, M.T.A.P. Kresnowati, I.G. Wenten, Electro-membrane processes for organic acid recovery, RSC

Adv. 9 (2019) 7854–7869. https://doi.org/10.1039/C8RA09227C.